Quaternary Science Reviews 321 (2023) 108356

Contents lists available at ScienceDirect

Quaternary Science Reviews

journal homepage: www.elsevier.com/locate/quascirev

Late Pleistocene–Holocene multi-decadal patterns of extreme floods in NW Iberia: The Duero River palaeoflood record

Gerardo Benito [a,*], Noam Greenbaum [b], Alicia Medialdea [c], Mikel Calle [d], Yolanda Sanchez-Moya [e], Maria Machado [a], Juan Antonio Ballesteros-Cánovas [a], Juan Pablo Corella [f]

[a] National Museum of Natural Sciences-CSIC, Serrano 115 bis, 28006, Madrid, Spain
[b] University of Haifa, 199 Aba Houshi Ave., Haifa, Israel
[c] National Research Centre on Human Evolution (CENIEH), Burgos, Spain
[d] Turku Collegium of Sciences Medicine and Technology (TCSMT), University of Turku, Finland
[e] Faculty of Geological Science, Complutense University of Madrid, Spain
[f] CIEMAT, Environmental Department, Madrid, Spain

ARTICLE INFO

Handling Editor: Dr C. O'Cofaigh

Keywords:
Palaeohydrology
Palaeofloods
Extreme floods
Palaeoclimate
North Atlantic Oscillation
Duero River
Spain
Portugal
Southern Europe

ABSTRACT

Extreme floods are anticipated to become more frequent in a future warmer climate. However, the long-term alterations in flood patterns across different regions of Europe remain unclear. In this study, we present a 15,000-year record of extreme floods in the Duero River, located in the southwestern Atlantic region. We analysed slackwater flood sediments, quantified the discharge and timing of individual flood beds over millennial time scales, and identified their potential climate influences. The composite record includes at least 62 floods grouped into ten flood-rich periods (with an average duration of 230 years). A high-frequency phase of moderate-magnitude floods (>10 events) occurred at ~11.6–11.5 ka, following a period of reduced flood activity during the Younger Dryas. Similar clusters of Early Holocene floods (10.8–10.3 ka, 9.5 ka) coincided with or preceded meltwater pulses from the North Atlantic. The absence of palaeoflood records with discharges exceeding 6100 m^3/s during the Mid-Holocene suggests a decline in winter hydro-meteorological extremes. High flood magnitudes were recorded during transition periods toward cooler and wetter conditions at 4.4, 2.3, 0.5, and 0.11 ka with discharges ranging from 7600 to 10,000 m^3/s. These periods were interpreted as indicative of a southward shift in cyclone tracks in Europe driven by negative phases of the North Atlantic Oscillation (NAO). Conversely, flood magnitudes decreased during past warmer climate conditions (1.7 ka, 0.9 ka, and the present), although flood frequency remained high. The current decline in flood frequency reflects an increase in flood regulation due to dams, but it is also consistent with the prevailing positive trend in the NAO observed over the last 40 years.

1. Introduction

Climate change is expected to modify future flood patterns on a global scale, though regional and local projections remain highly uncertain (Jiménez Cisneros et al., 2014; Kundzewicz et al., 2014). This uncertainty is amplified when it comes to rare and extreme floods, as their infrequency often exceeds the duration of instrumental hydrological records (Baker et al., 2022). Notably, recent unprecedented catastrophic floods are now referred to as super-extreme floods in the context of climate change. For instance, the exceptional flood on the River Ahr in Germany in July 2021 was four to five times larger than the largest recorded flood since 1946 (Mohr et al., 2022). However, the magnitude and spatial extent of the 2021 flood were similar to the pre-instrumental July 1804 flood, as estimated from historical markers (Roggenkamp and Herget, 2014, 2022).

Hence, the perception of an extraordinary flood event depends on the temporal scale and socio-economic impacts, with the latter often associated with increased human settlement density in flood-prone areas in recent decades. The 2021 flood serves as an illustration of the importance of understanding extreme event patterns from a long-term

* Corresponding author.
E-mail addresses: benito@mncn.csic.es (G. Benito), noamgr@geo.haifa.ac.il (N. Greenbaum), alicia.medialdea@cenieh.es (A. Medialdea), mcanav@utu.fi (M. Calle), yol@ucm.es (Y. Sanchez-Moya), mjmachado09@gmail.com (M. Machado), JuanPablo.Corella@ciemat.es (J.P. Corella).

https://doi.org/10.1016/j.quascirev.2023.108356
Received 16 July 2023; Received in revised form 6 October 2023; Accepted 12 October 2023
Available online 27 October 2023

perspective, beyond their multi-decadal variations. In this regard, information gleaned from past floods has become a crucial source of data for quantifying the connections between extreme event patterns, long-term frequency analysis, natural climate variability, and, therefore, for anticipating future climate change impacts (Baker et al., 2022).

Long-term palaeoflood datasets can be derived from a variety of natural archives, including lake sediments (e.g., Corella et al., 2016; Schillereff et al., 2016; Wilhelm et al., 2019; Corella et al., 2021), speleothems (e.g., Denniston and Luetscher, 2017; Feinberg et al., 2019; Gonzalez-Lemos et al., 2015), botanical evidence (Yanosky and Jarrett, 2002; Ballesteros-Cánovas et al., 2015), and fluvial deposits (Baker, 1987; Greenbaum et al., 2014). Sedimentary records from lakes, speleothems, or botanical evidence can provide continuous flood records, although they certainly pose challenges when attempting to derive quantitative discharge data for specific floods (Ben Dor et al., 2018; Noren et al., 2002; Wilhelm et al., 2018) or when they are limited in time to the last few centuries (Wilhelm et al., 2019). In contrast, flood beds deposited in bedrock fluvial reaches with stable and confined geometries are well-suited for quantitative long-term flood discharge estimates based on stage-discharge relationships (Baker and Kochel, 1988; Benito et al., 2020). However, fluvial palaeoflood records can exhibit bias toward recent times due to erosion caused by rare and extreme floods (Baker, 2008; Lewin and Macklin, 2003).

A major limitation in palaeoflood hydrology studies lies in the preservation of long-term depositional evidence. In confined rivers, flood deposits typically occur in discontinuous overbank sequences (benches), sediment pockets on slopes and within rock shelters with a limited number of flood beds. Furthermore, the preservation of flood sediments in fluvial systems depends on the climatic, geological and physiographic regional context which in turn influences the type of the information and the temporal extent of the record (O'Connor et al., 2002). As a result, only in a few rivers worldwide have been documented continuous and homogeneous flood records spanning the last glacial termination and current interglacial period (e.g., Benito et al., 2003b; Ely et al., 1996; Enzel, 1992; Li and Huang, 2017; Liu et al., 2015; Sridhar, 2007; Yang et al., 2000; Zhou et al., 2016). Reconstructing hydrological extremes within specific river basins provides a foundation for a robust and consistent characterisation of flood responses to climate, both temporally and spatially. Such analogues play a critical role in understanding recent and future flood patterns in the context of global change (Benito et al., 2021; Baker et al., 2022).

The analysis of extensive fluvial databases has enabled the reconstruction of long-term Holocene fluvial dynamics in Europe (Macklin et al., 2006; Jones et al., 2015). Through meta-analyses, the spatial and temporal distribution of flood-rich periods has been attributed to changes in atmospheric circulation patterns (e.g., Benito et al., 2015b). In the southwestern European region, existing flood records suggest that flood-rich periods coincided with transitions to cooler and wetter conditions, leading to a southward shift of westerlies (Benito et al., 2015c). These atmospheric conditions are primarily influenced by the North Atlantic Oscillation (NAO), which relates to the distribution of high and low sea level pressure between the Azores and Iceland (Hurrell, 1995). During winter, a negative NAO phase signifies a reduced pressure difference between the Icelandic low and the Azores high, resulting in weaker westerly winds and a southward shift of cyclonic tracks towards the Iberian Peninsula (Salgueiro et al., 2013; Trigo et al., 2004a). This negative NAO phase typically coincides with the occurrence of winter blocking episodes in the North Atlantic, featuring a pronounced surface air temperature anomaly characterized by a "warm ocean/cold land" pattern (Shabbar et al., 2001; Trigo et al., 2004b). In contrast, a positive NAO phase implies stronger westerly winds and a cyclonic circulation that brings wetter conditions to northern Europe and drier weather to southwestern Europe (Trigo, 2006). The variability in NAO explains the spatial distribution of precipitation, seasonal river discharge, and flood occurrence across much of western Europe (Hurrell, 1995; Stanev and Peneva, 2001; Rimbu et al., 2002; Trigo et al., 2004a; Lorenzo-Lacruz et al., 2011; Benito et al., 2015b,c).

Previous studies have identified persistent modes of NAO phase (positive or negative) on decadal, interdecadal, centennial, and even millennial time scales (e.g., Hurrell, 1995; Visbeck et al., 2001; Trouet et al., 2009; Baker et al., 2015). Various forcing mechanisms have been proposed to explain this non-stationarity, including changes in the meridional pressure gradient (Zveryaev, 2006), the strength of the thermohaline circulation (Thornalley et al., 2009), variations in solar activity (Gimeno et al., 2003), and meltwater pulses and their feedback with the NAO (Olsen et al., 2012). These longer-term variations in the NAO have significant implications for climate and weather patterns in the North Atlantic region and beyond (see section 5.4).

While analyses based on fluvial metadata have provided valuable insights into long-term flood-climate relationships in Europe (e.g., Macklin et al., 2006; Benito et al., 2015c), they suffer from discontinuity and temporal constraints, leaving a gap in our understanding of multi-decadal to centennial flood responses to climate in large river basins. Therefore, local records of extreme floods within large river catchments are essential to identify changes in weather patterns that lead to floods over multiple natural climate cycles, such as extratropical cyclones and atmospheric rivers. This knowledge would provide a high level of confidence in predicting which climate modes might trigger catastrophic floods in near-future scenarios.

In this context, we present a 15,000-year record of extreme floods in one of the largest river catchments in southern Europe, the Duero/Douro River. Our study includes the reconstruction of peak discharge and the timing of individual flood events over millennial time scales. We complemented sedimentary evidence from slackwater flood deposits (SWDs) with available pre-instrumental data covering the last 500 years, including flood marks and descriptive accounts of past flood levels (Iberduero, 1953, 1956; Silva and Oliveira, 2002; Benito et al., 2021). Building upon this analysis, we aim to contribute to the ongoing discussion on flood-climate relationships by addressing the following research questions:

(a) What is the impact of centennial-scale climate variability (warm/cold) on flood magnitude and frequency?
(b) What are the potential paleoclimate drivers, and how do they influence centennial to millennial flood patterns?
(c) Can we use past hydroclimatic periods during the Holocene as analogues for near-future scenarios within the context of a warming climate?

2. Study area

2.1. Duero River catchment

The Duero is one of the three major rivers of the Iberian Peninsula flowing east-west for 897 km from the Spanish plateau into the Atlantic Ocean at Porto (Portugal). It is the largest river in the Iberian Peninsula in terms of catchment area (98,074 km^2), of which 78,859 km^2 are in Spain (~80%) and 19,215 km^2 in Portugal (Fig. 1). Most of the rainfall is produced by Atlantic frontal depressions from November to April. On the western side, the orographic effect and the influence of the ocean on the climate produce an average annual rainfall of 1175 mm in the lower Douro (Portugal). In the Spanish Duero basin, the mean annual rainfall is 580 mm, with a high inter-annual variation of 350 mm–800 mm (+/−40%). Similarly, the maximum daily rainfall on the Portuguese Douro catchment can reach 200 mm, while in the Spanish Duero it varies between 60 and 100 mm.

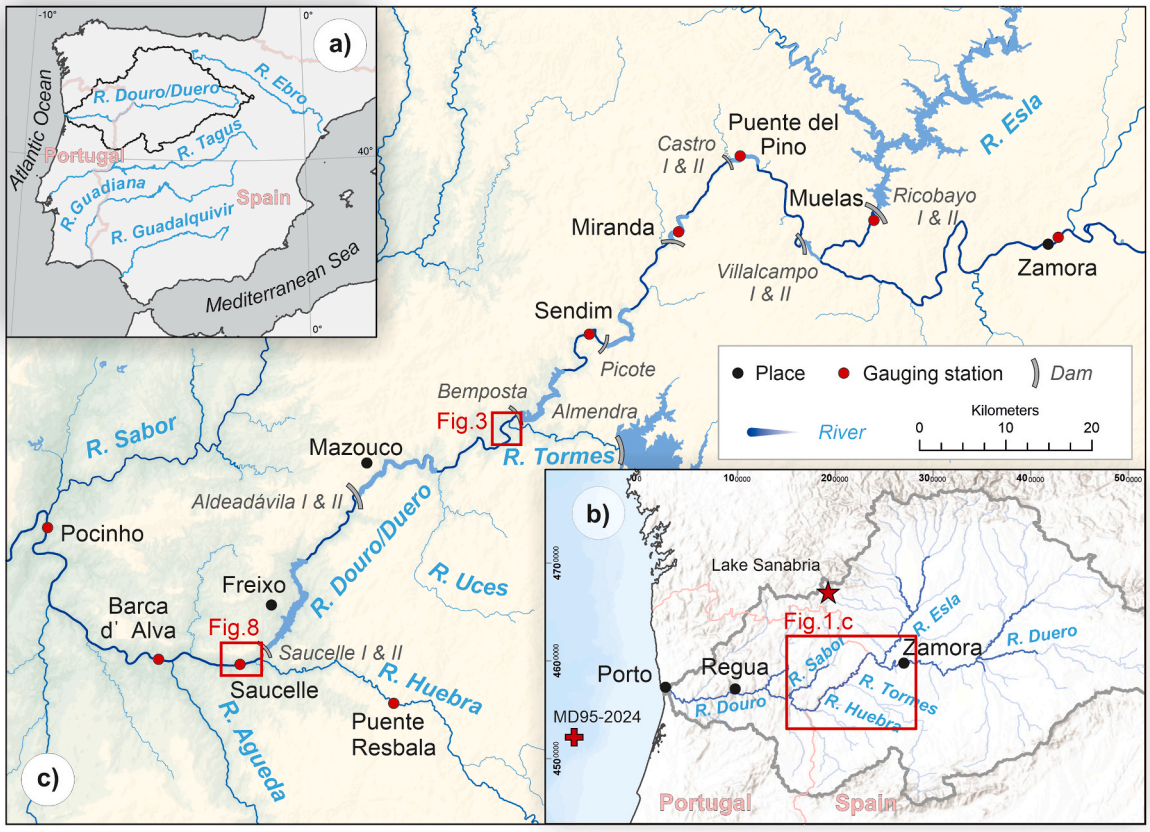

Fig. 1. a) Location map of the Duero River catchment within the Iberian Peninsula and the other major river basins draining to the Atlantic Ocean. b) Relief map of the NW Iberian Peninsula and the boundary of the Duero catchment, the main river network and cities. The rectangle shows the location of (c). c) Hillshade map of the international section of the Duero/Douro River along the border between Spain and Portugal. The study reaches are located (1) downstream of the Bemposta dam and (2) downstream of the Saucelle dam. Also shown are the locations of gauge stations and sites with important hydroclimatic proxy records, Lake Sanabria (Jambrina-Enríquez et al., 2014, 2016) and marine core MD95-2040 at the Iberian margin (de Abreu et al., 2003).

Geologically, the Duero catchment comprises two regions. The eastern (Spanish) sector is formed by detrital and evaporitic rocks corresponding to the Cenozoic continental basin (~50,000 km^2, Alonso-Zarza et al., 2002). This basement is covered partially by Quaternary alluvial fans and fluvial terraces, with a stair-like landscape resulting from episodic river incision after the onset of the exoreic basin conditions (Martin Serrano, 1991; Rodríguez-Rodríguez et al., 2020). The western sector (Spanish-Portuguese fringe and Portuguese domain) is composed of Palaeozoic metamorphic and granitic basement rocks, where the river network is entrenched, forming confined fluvial valleys. Downstream of Zamora, the Duero River flows along a 120 km long canyon deeply incised up to 500 m into the adjacent peneplain, a polygenic erosional surface dated to the end of the Miocene (Marino Alfonso et al., 2018). The Duero River bedrock canyon forms the boundary between Spain and Portugal for 112 km and the Duero/Douro International Natural Park, also known as Los Arribes in Spain (Fig. 1). The confluences of three major tributaries, the Esla, Tormes and Agueda rivers, are located along this international stretch.

The incision of the Arribes canyon has been interpreted as a diachronous process (Martin-Serrano, 1991) that started during the Late Miocene-Early Pliocene in a post-orogenic context, when the Cenozoic continental basin became connected to the Atlantic Ocean (Santisteban et al., 1996). An examination of longitudinal profiles within the Duero drainage network (Struth et al., 2019) reveals a significant knickpoint at 655 m above sea level (a.s.l.) at the entrance to the Arribes canyon. This knickpoint divides the catchment into a mid-lower western section with minor knickpoints (proto-Duero) and an upper eastern section that extends over the Cenozoic sedimentary infill.

According to Antón et al. (2012), the bottom 200–300 m of fluvial incision in the lower Arribes canyon occurred at an average rate of 2–3 m/ka over the last ~100 ka, as determined by cosmogenic exposure dating. Note that cosmogenic exposure dating assumes no post-fluvial erosion of the dated surfaces, so the calculated exposure age represents a minimum age, and the incision rate reflects a maximum rate (Schaller et al., 2016). Downstream of the Arribes canyon (at Pocinho, see Fig. 1), Cunha et al. (2019) derived a mean incision rate of 1.40 m/ka based on two OSL dates from the younger T1 alluvial terrace (~13 ka). In the Tormes River, within the Cenozoic basin in Salamanca, Goy et al. (2019) calculated incision rates of 0.08 and 0.25 m/ka for the Late Pleistocene and Holocene periods, respectively. In section 5.1, we describe the evidence for channel incision within our study reach, and discuss about the implication of the river incision in the palaeoflood discharge estimates.

2.2. Modern flood hydrology

Duero River floods typically are associated with persistent winter rainfall (days to weeks), combined with snowmelt from tributaries draining the high mountain reliefs of the Gredos (Central System) and the Cantabrian Mountains. The contrasting rainfall patterns between the Spanish Duero and the Portuguese catchment sectors give rise to large differences in the flood hydrographs and flood peaks along the international Duero/Douro reach, producing a clear inflection point at the lower stations (Fig. 2b). For example, the 1962-flood recorded a peak of 15,700 m^3/s at Régua, Portugal (Silva and Oliveira, 2002), whereas at Zamora (Villachica station, Spain), just upstream of the Duero gorge, the

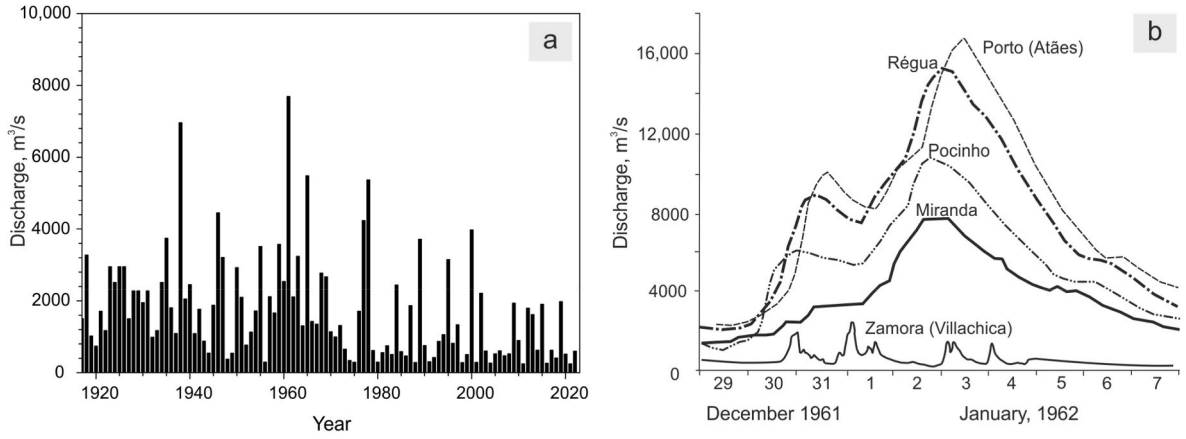

Fig. 2. a) Annual daily maximum discharges (1917–2022) of the Duero River upstream of the Tormes River confluence compiled from Puente del Pino, Miranda and Sendim gauge stations (see locations in Fig. 1). b) Hydrographs of the 1962-flood at different gauge stations along the river. Note the sharp increase in flood peak and volume in Miranda at the Duero/Douro gorge and along the downstream locations (Pocinho, Régua and Porto) (after Daveau, 1988).

discharge was only 1730 m^3/s (Benito et al., 2021). The peak discharges of the Duero, recorded at Porto and Régua, are among the highest absolute largest discharges of European rivers (Benito et al., 2015a; Pardé, 1967). High discharge is explained by a combination of factors, including the advection of humid air masses penetrating inland, mountainous relief that reduces the concentration time, and impervious geology (igneous and metamorphic rocks). In contrast, the Duero River in Spain flows through an open valley with a well-developed floodplain and underlying detrital carbonate lithology. Thus, there is a significant contrast in flood volume between these regions, with peak flows increasing along the International Douro/Duero River canyon where several major tributaries (Esla, Huebra and Tormes) converge. In the upper International Duero sector, the maximum flood discharges in the instrumental record (1917–2022) from Puente del Pino (Spain), Miranda do Douro and Sendim (Portugal) were 6960 m^3/s in 1939 and 7300 m^3/s in 1962 (Fig. 2a). A previous large historical flood occurred in 1909 with an estimated discharge of 7700 m^3/s.

2.3. Documentary floods

The most complete historical flood archives of the Duero River have been documented in the urban areas of Zamora (Spain), Régua, Vila Nova de Gaia and Porto (Portugal). In Zamora, 69 flood events have been documented for the period 1511–1871 (Benito et al., 2021). The temporal distribution of floods shows a number of periods of increased flood frequency, namely during 1600–1640, 1730–1750, 1770–1790 and 1880–1910. In the 20th century (gauge records spanning 1917–2023), the frequency of extraordinary floods increased in the period 1935–1966. In Zamora, the largest floods of the last 500 years occurred in 1860 (3450 m^3/s), 1597 (3200 m^3/s), and 1739 (2700 m^3/s). These flood discharges were greater than those recorded in the early gauge readings (Porvenir station, largest in 1895–2380 m^3/s) and in the Carrascal (Zamora) gauging station (largest in 1960–2360 m^3/s).

In the lower Douro River in Portugal documentary floods have been reported mainly in Régua and Porto (Aires et al., 2000; Alcoforado et al., 2021; Amorim et al., 2017; Loureiro, 1904). In Régua, Silva and Oliveira (2002) compiled flood levels and estimated discharges of extreme floods since 1727, the largest one occurred in 1739 with a discharge of 18,000 m^3/s. In Porto the 1739 flood was estimated at 19,000 m^3/s (Daveau, 1988). The second and the third largest recorded floods are those of Dec. 1909–16,700 m^3/s and the Jan. 1962–15,700 m^3/s, respectively, with flood depths of 20–25 m in Régua and 10–12 m in Porto (Daveau, 1978; Silva and Oliveira, 2002). Flood-rich periods have been identified in the periods 1770–1790 and 1850–1880, dominated by generally wet winter years (Alcoforado et al., 2021; Amorim et al., 2017).

2.4. Synoptic weather conditions linked to extreme precipitation and flooding

Synoptic weather patterns leading to extreme rainfall in the Duero catchment are closely linked to the presence of an intense cyclonic anomaly, which typically extends into the mid-Atlantic Ocean (Cortesi et al., 2013). The cyclonic trajectory toward southern Atlantic Europe tends to occur during negative phases of the North Atlantic Oscillation (Lorenzo-Lacruz et al., 2011; Trigo, 2006), as well as during winter blocking episodes that alter the jet stream and the location of maximum cyclonic activity (Trigo et al., 2004a). Additionally, many of the most substantial peak flows observed in Iberian Atlantic catchments are associated with the influence of intense atmospheric rivers (ARs). These are transient and narrow corridors, approximately 300 km wide, responsible for transporting poleward water vapor ahead of the cold front of an extratropical cyclone (e.g., Ballesteros-Cánovas et al., 2019; Liberato et al., 2013; Ramos et al., 2015; Trigo et al., 2014). For instance, catastrophic floods such as those in December 1909 in the Duero River (Benito et al., 2021; Pereira et al., 2016) and December 1876 in the Guadiana River (Trigo et al., 2014) were triggered by episodes of atmospheric rivers over the North Atlantic sector.

2.5. Study reaches

The international reach of Duero-Douro River is characterized by a 3 m/km channel slope to connect the Cenozoic Duero Basin with the Portuguese lowlands. This bedrock canyon contains seven dams built between 1940 and 1960. We selected two study reaches in the International Duero River located between the dam wall and the tail of the downstream reservoir (Fig. 1).

The 7 km long Bemposta reach is located between the Bemposta dam (Portugal) and the tail of the Aldeadavila reservoir, next to Vilariño (Spain). In this reach, the Duero River drains a catchment area of 70,960 km^2. Here, the Duero River valley is cut into the bedrock, forming an escarped canyon with a depth of ~200-m and a width of 45–135 m. The Bemposta reach is constricted in its most downstream sector, creating a backwater effect on the upstream valley expansions.

Slackwater flood deposits have accumulated in these canyon expansions, including the widest one at the Tormes River confluence, with space for deposition and long-term preservation conditions for these sedimentary features. The slopes of the Duero valley are cultivated, with olive trees on the Portuguese side, whereas the Spanish slopes are mostly covered with shrubs and scattered trees. Nevertheless, in the past the Spanish region was also known for the extensive cultivation of vinyards on gentle slopes and olive trees on steep slopes (Morán-Tejeda et al.,

2012).

The Saucelle reach is 1.3 km long and is located between Saucelle (Spain) and Freixo (Portugal), 400 m downstream of the confluence of the Huebra and Duero rivers (Fig. 1). Here the Duero River drains a catchment area of 75,031 km^2, and the river channel is 150 m wide, entrenched in a 300 m deep bedrock canyon. Most of the palaeoflood sediments are deposited on the left margin (Spanish side), forming a narrow bench in the lee side of a granite outcrop.

3. Data sources and methods

3.1. Documentary and historical gauged records

A compilation of the largest documentary floods was obtained from published datasets, namely at Zamora (Benito et al., 2021), Régua (Silva and Oliveira, 2002) and Porto (Alcoforado et al., 2021; Amorim et al., 2017; Daveau, 1978). In the study reaches, flood water levels were documented from technical reports related to the Saucelle and Aldeadávila dams (Iberduero, 1953, 1956). The epigraphic marks (flood levels) and description of the areas affected by flooding from these reports allow estimation of a relative magnitude of the largest historical floods and/or the peak discharge for specific floods at the study sites.

3.2. Palaeoflood stratigraphy

Aerial photography and field reconnaissance allowed the identification of the best sections for detailed stratigraphic and sedimentological descriptions to compile palaeoflood records. Slackwater flood deposits were preserved in stratigraphic sequences within benches on the valley sides the elevations of which were used as palaeostage indicators (Kochel and Baker, 1982). Detailed stratigraphic description and sampling for geochronological and textural analysis were carried out on 13 stratigraphic profiles along the Bemposta reach, and two profiles in the Saucelle reach. The descriptions were made for wide exposures, mostly excavated by backhoe or by shovel. Individual flood units were recognised by a variety of sedimentological indicators (Baker and Kochel, 1988; Benito et al., 2020) separating flood units, namely clay laminae at the top of a flood bed, erosive contacts, bioturbation indicating the exposure of a sedimentary surface, buried paleosols, clast from the slope, and changes in sediment colour. Sedimentary flow structures have been described in the flood-beds to elucidate the local flow dynamics during a particular flow event.

3.2.1. Palaeoflood chronology

The palaeoflood chronology was established from 37 Optically Stimulated Luminescence (OSL) dated sand samples (Table 1) and one radiocarbon date obtained for individual flood units. OSL dating analyses were carried out in two laboratories: (1) the Radioisotope Unit of the University of Seville, and (2) the OSL dating facilities of the University of Cologne. Samples were collected in the field using PVC tubes to avoid exposure of the sediment to light. The AMS ^{14}C dating was carried out at the Spanish Accelerator Centre in Seville (CNA). Radiocarbon ages were calibrated to calendar ages using Oxcal 4.4 software (Ramsey, 2001) based on the IntCal20 calibration data set (Reimer et al., 2020).

Quartz grains with a size range of 180–250 μm were extracted from

Table 1
Summary of total dose rates, estimated equivalent doses derived from the OSL measurements and the resulting ages. Geographical coordinates and sampling depth of each sample are also given. Abbreviations used in the text: Cicutina (Ci), Dos Olivos (Do), Enebro (En), Fox (Fo), Morera (Mo), Muga (Mu), Tabanera (Ta), Teso (Te), Tormes (To), Vilariño (Vi).

Sample	Longitude	Latitude	Depth (m)	Dose rate (Gy/ka)	Equivalent dose (Gy)	Age (ka)
MUGA-1	−6.478788	41.292863	2.7	3.43 ± 0.10	47.4 ± 1.5	**13.8 ± 0.6**
MUGA-3	−6.478788	41.292863	2.1	3.51 ± 0.10	29.3 ± 1.3	**8.4 ± 0.4**
MUGA-5	−6.478788	41.292863	1.3	3.13 ± 0.09	7.4 ± 0.3	**2.4 ± 0.1**
TORMES-1	−6.478347	41.293229	3.45	2.69 ± 0.08	31.3 ± 0.6	**11.6 ± 0.4**
TORMES-5	−6.478347	41.293229	2.85	2.42 ± 0.07	27.8 ± 0.8	**11.5 ± 0.5**
TORMES-7	−6.478347	41.293229	2.3	2.39 ± 0.08	22.6 ± 0.7	**9.5 ± 0.4**
TORMES-12	−6.478347	41.293229	1.65	2.17 ± 0.06	20.5 ± 0.7	**9.5 ± 0.4**
TORMES-14	−6.478347	41.293229	1.3	2.48 ± 0.07	22.8 ± 0.6	**9.2 ± 0.4**
TORMES-17	−6.478347	41.293229	0.8	2.98 ± 0.09	13.2 ± 0.5	**4.4 ± 0.2**
TORMES-22	−6.478347	41.293229	0.4	3.08 ± 0.15	6.6 ± 0.5	**2.1 ± 0.2**
TABANERA-2	−6.478657	41.293153	4.6	2.41 ± 0.09	35.9 ± 1.0	**14.9 ± 0.7**
TABANERA-5	−6.478657	41.293153	3.5	2.45 ± 0.09	30.9 ± 1.2	**12.6 ± 0.7**
TABABANERA-12	−6.478657	41.293153	2.1	3.08 ± 0.12	35.6 ± 1.1	**11.5 ± 0.6**
CICUTINA-3	−6.478499	41.293218	3.7	3.02 ± 0.13	35.0 ± 0.9	**11.6 ± 0.6**
CICUTINA-7	−6.478499	41.293218	2.4	2.69 ± 0.12	33.5 ± 1.6	**12.4 ± 0.8**
CICUCUTINA-12	−6.478499	41.293218	1.2	2.76 ± 0.10	32.7 ± 1.9	**11.8 ± 0.8**
CICUTINA-16	−6.478499	41.293218	0.5	3.32 ± 0.16	34.9 ± 1.3	**10.5 ± 0.6**
FOX-1	−6.485053	41.281784	2.5	3.84 ± 0.12	39.6 ± 2.3	**10.3 ± 0.7**
FOX-6	−6.485053	41.281784	0.6	3.20 ± 0.14	9.3 ± 0.6	**2.9 ± 0.2**
ENEBRO-6	−6.492020	41.288314	1.7	2.45 ± 0.11	3.2 ± 0.1	**1.31 ± 0.07**
ENEBRO-12	−6.492020	41.288314	2	3.13 ± 0.10	3.2 ± 0.2	**1.02 ± 0.07**
ENEBRO-14	−6.492020	41.288314	1.7	2.82 ± 0.12	2.7 ± 0.1	**0.95 ± 0.05**
ENEBRO-17	−6.492020	41.288314	1.2	3.56 ± 0.16	2.7 ± 0.1	**0.77 ± 0.04**
ENEBRO-19	−6.492020	41.288314	1	3.59 ± 0.15	1.9 ± 0.1	**0.53 ± 0.03**
ENEBRO-21	−6.492020	41.288314	0.7	3.85 ± 0.13	1.9 ± 0.1	**0.50 ± 0.03**
TESO 2-1	−6.492828	41.287276	0.7	3.83 ± 0.18	6.9 ± 0.2	**1.8 ± 0.1**
VILARIÑO-3	−6.480720	41.277510	1.2	3.02 ± 0.10	1.67 ± 0.09	**0.55 ± 0.04**
DOS OLIVOS-1	−6.814657	41.033465	0.5	3.59 ± 0.15	1.15 ± 0.08	**0.32 ± 0.02**
DOS OLIVOS-2	−6.814657	41.033465	0.6	3.78 ± 0.16	1.44 ± 0.06	**0.38 ± 0.02**
DOS OLIVOS-3	−6.814657	41.033465	1.2	3.44 ± 0.14	2.82 ± 0.13	**0.82 ± 0.05**
DOS OLIVOS-4	−6.814657	41.033465	1.5	2.85 ± 0.11	2.64 ± 0.07	**0.93 ± 0.04**
DOS OLIVOS-5	−6.814657	41.033465	1.8	3.09 ± 0.13	3.20 ± 0.11	**1.04 ± 0.06**
MORERA-4	−6.814021	41.033991	0.6	3.65 ± 0.15	1.91 ± 0.05	**0.52 ± 0.03**
MORERA-6	−6.814021	41.033991	1	2.52 ± 0.10	2.91 ± 0.08	**1.16 ± 0.06**
MORERA-8	−6.814021	41.033991	2	2.88 ± 0.12	4.31 ± 0.11	**1.50 ± 0.07**
MORERA-11	−6.814021	41.033991	2.8	3.04 ± 0.13	5.37 ± 0.11	**1.77 ± 0.08**
MORERA-12	−6.814021	41.033991	3.2	2.85 ± 0.12	6.37 ± 0.18	**2.23 ± 0.11**

the selected samples for OSL measurements. The doses accumulated during the burial time (equivalent doses) were measured in 40–70 small aliquots of several grains from each sample. These aliquots, each containing <20 grains, had sufficient resolution to detect extrinsic effects such as incomplete bleaching (Medialdea et al., 2014). Luminescence measurements were performed using an automated Risø OSL/TL reader (TL-DA 20) with a calibrated $^{90}Sr/^{90}Y$ beta source. Dose recovery tests were used to determine the most appropriate measurement settings and to verify the suitability of the method to accurately recover a given dose (Medialdea et al., 2014). Equivalent doses were estimated from the dose distributions using the Central Age Model (Galbraith et al., 1999). Data were reduced to limit the scatter in the dose distributions by removing outliers after 1.5 times the interquartile range determined for the box plots (Tukey, 1977). The dose populations were normally distributed, except for samples DOL-1 and DOL-2, which show a tail of high doses. This tail is most likely an indication of incomplete bleaching of the quartz grains. In these two samples we applied an IEU (Internal-External Uncertainty Criterion) minimum age approach (Thomsen et al., 2007).

Beta and gamma dose rates were obtained from the radionuclide activity concentration derived from high-resolution gamma spectrometry measured in ~100 g of bulk material from the sediment matrix of each sample. The contribution of cosmic radiation was calculated according to a variable burial depth (Prescott and Hutton, 1994). Final dose rates were calculated using DRAC (Dose rate and age calculator; Durcan et al., 2015). Sampling depths, total dose rates to an infinite matrix, and the derived age estimates are shown in Table 1.

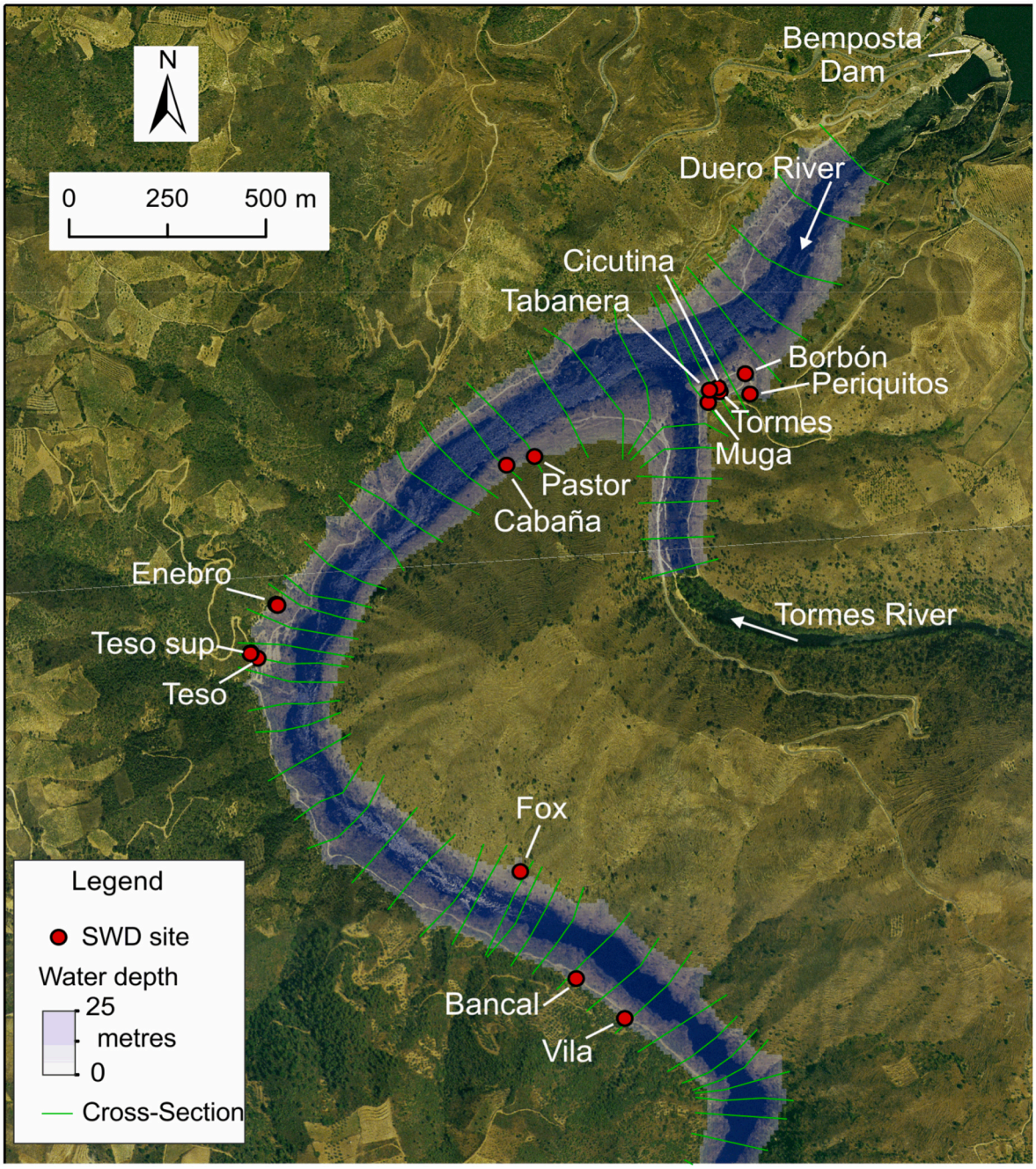

Fig. 3. Orthophotograph of the Bemposta reach (year 2017) showing the locations of the stratigraphic profiles described in the text and the valley cross-sections used in the one-dimensional hydraulic model (HEC-RAS). The cross sections are presented on the 2 m grid DTM generated from Lidar data (provided by the Spanish National Geographic Institute (IGN; https://www.ign.es, last accessed: 4 May 2023) in ArcGIS. The water depths correspond to a modelled discharge of 11,000 m^3/s.

3.2.2. Discharge estimation

The estimation of paleoflood discharges is based on the premise that (1) the elevation of the top of a flood unit represents the minimum flood stage reached by the flood, and (2) the topographic changes of the study reach are minimal. In order to quantify the uncertainties in the estimation of peak discharge associated with long-term incision at the study site, we carried out a detailed field inspection to identify strath surfaces cut into the bedrock. Assuming that these strath surfaces represent the former bed level of the river channel, probably during the Holocene, we used the bathymetric survey to quantify the excess cross-sectional area and its effect on peak discharge.

The palaeoflood stage of each flood stratigraphic unit was used to estimate the minimum discharge through hydraulic modelling. The computations were performed using the one-dimensional hydraulic - HEC-GeoRAS v.5 model (Hydrologic Engineering Center, 2010). The terrain topography was reconstructed from a 2-m grid produced from LiDAR data provided by the Spanish National Geographic Institute (IGN; https://www.ign.es). The topography of the river bed and banks was obtained from field bathymetric surveys and topographic maps (1:2000) included in the Aldeadávila dam engineering project report (Iberduero, 1956). The topographic maps were digitised on the basis of identified reference points with known coordinates. Bathymetric points from 21 cross sections (~350 m apart) were interpolated and integrated with the LiDAR DTM using the Spatial Analyst tools in ArcGIS v.10. The HEC-GeoRAS model consisted of 70 cross sections along the Duero River and six cross sections in the Tormes River (Fig. 3). The initial Manning's *n* values used in the modelling were assigned from land use map classes (Corine Land Cover map) according to the methodological guide of the Spanish Flood Inundation Hazard Map (MMA, 2011). The initial *n* values were validated based on field water surface elevations of known gauged discharges, including the height of the 2001 flood. Manning's *n* values were set to 0.0312 for the channel, 0.0562 for the exposed bedrock (rough), 0.0480 for the scattered vegetated surface and 0.0650 for the densely vegetated surface. A sensitivity test was carried out for a 25%

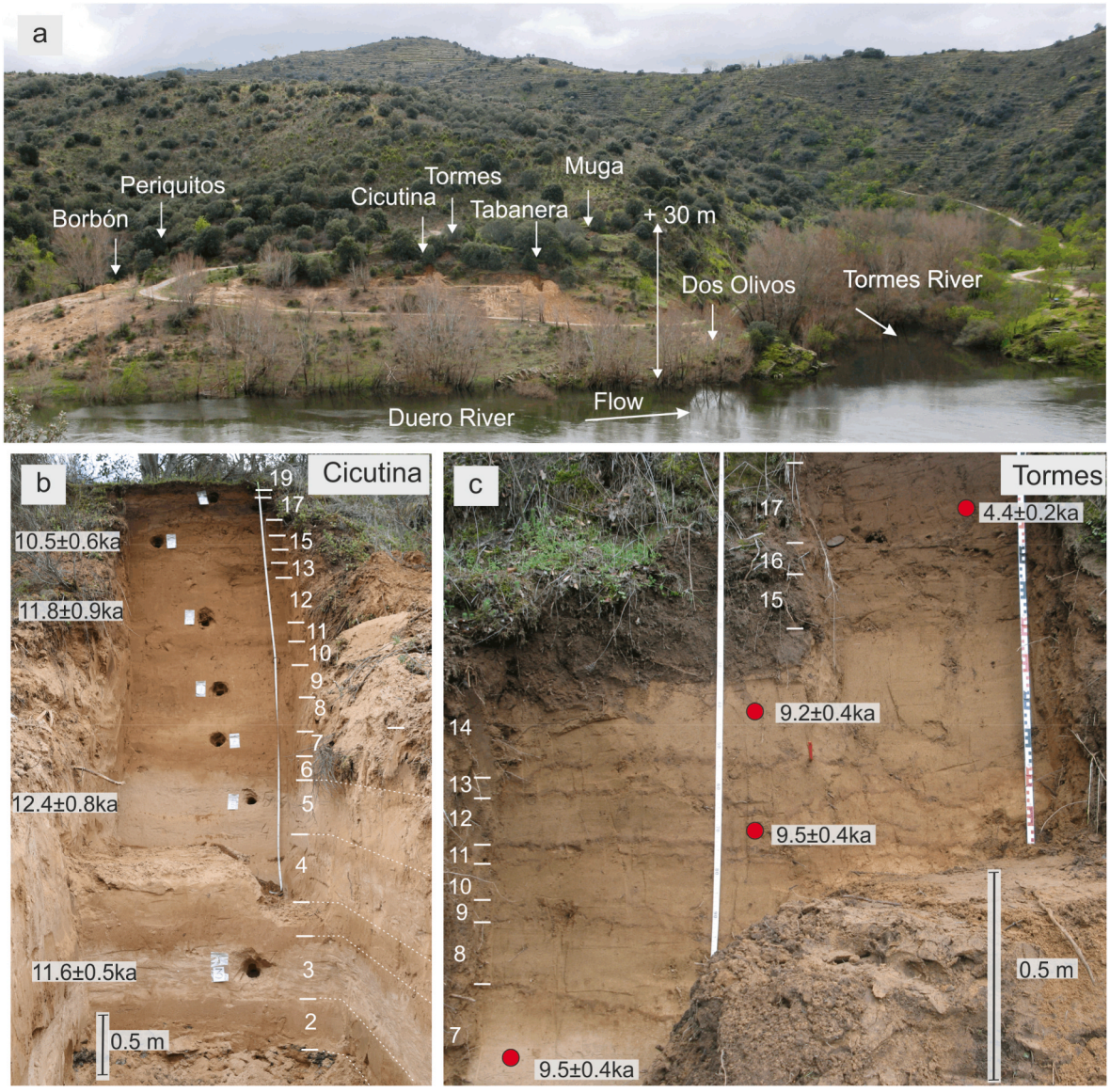

Fig. 4. Photographs from the upper Bemposta reach. a) View towards the Duero-Tormes confluence with SWD bench surfaces and location of stratigraphic profiles. Note that the highest flood sediments reach 30 m above the river level. b) Sequence of 19 flood beds in the Cicutina profile and depths of OSL dating samples. Note the OSL age of 11.6 ka underneath ages of 12.4 ka and 11.8 ka, suggesting incomplete bleaching of the later samples. c) Detailed section of sandy flood beds in the Tormes profile, consisting of two sub-sequences differentiated by their colour - light brown vs. dark brown, dated in the early and Late Holocene, respectively. Note the horizontal contacts in the lower sequence formed by reddish clay-silt laminae at the boundaries of the flood layers.

variation in roughness values, indicating an error of 4–8 % introduced into the discharge calculations. Model calibration was performed using: (a) water surface elevation values along the canyon, initially based on elevation data reported in the dam technical report for a discharge of 150 m^3/s, and (b) water level field surveys (May 2018) at a known discharge. The palaeoflood sites and documented historical flood levels were surveyed using a Trimble differential GPS, supported by three geodetic survey monuments from the Spanish Geographic Institute and the Bemposta dam.

4. Results

4.1. Palaeoflood geomorphology and stratigraphy

In this section we first describe the stratigraphy and chronology of flooding events in the key stratigraphic sections of the two study reaches (sections 4.1), followed by their discharge quantification using hydraulic modelling (section 4.2).

4.1.1. Bemposta-Vilariño reach

Slackwater deposits (SWD) along the Duero River are preserved in thick, high-standing benches in canyon expansions and tributary mouths. Twelve high-resolution stratigraphic profiles were studied. Flood deposits were dated using optically stimulated luminescence (OSL) dates, and one radiocarbon date, covering the last 15 ka (Fig. 3).

The most complete record is found at the Duero-Tormes river confluence, which comprises four inset SWD benches at elevations between 15 and 30 m above the mean river water level (a.r.l.). The oldest bench (second in height) is 3–4 m thick and consists of multiple flood beds, each is well marked by horizontal to undulating, though conformable, contacts (Cicutina and Tabanera profiles; Fig. 4a). The Tabanera profile contains at least 17 flood beds, while the Cicutina profile (2 m higher) contains 19 floods (Fig. 4b and 5). The lower flood units (30–50 cm thick) consist of fine to medium pale sand with current ripples, indicating upstream flow direction, whereas the middle-upper flood beds (15–30 cm thick) are dominated by reddish fine to very fine, massive sand with frequent bioturbation marks. In these profiles, the repeated flood bedding is interrupted by occasional buried soils formed during periods of flood quiescence or small floods (Fig. 5). In the Tabanera profile, the oldest flood bed (Ta-02) was OSL dated at 14.9 ± 0.7 ka, overlain by seven flood beds (Ta-03 to Ta-09) dated between 12.6 ± 07 and likely 12.4 ± 0.8 ka (Ci-07), and by two flood beds (Ta-10 to Ta-11) with an age of ~11.5 ± 0.6 ka (Fig. 5). The upper flood cluster at Tabanera (Ta-12 to Ta-17) was laterally correlated with Cicutina (Ci-12 to Ci-19), which was OSL dated at 10.5 ± 0.6 ka (Ci-16).

In a higher flood bench, the Tormes profile is ~4 m thick and contains at least 23 flood beds within three sets separated by unconformities (Fig. 4c and 5). The lower five units (To-01 to To-05) consist of 10–15 cm thick beds of yellowish and reddish, fine to medium sand highly bioturbated and with edaphic features (nodules). The upper bed of this flood sequence (To-05) contains a well-developed reddish paleosol (Bt horizon; Fig. 5). Flood beds To-01 and To-05 were OSL dated to 11.6 ± 0.4 ka and 11.5 ± 0.5 ka, respectively (Fig. 5), correlating in time with the Ta-10 to Ta-11 flood beds. The second set of floods (To-06 to To-14) comprises nine flood units (5–20 cm thick) composed of yellowish fine to very fine sand, with contacts well marked by 1–5 cm thick reddish silt and clay laminae (Fig. 5c). Flood beds To-07 and To-14 were OSL dated to 9.5 ± 0.4 ka and 9.2 ± 0.4 ka, respectively (Table 1). The upper flood set contains nine flood beds with the lowest contact separated by an erosive unconformity with root marks. The flood beds are 3–22 cm thick

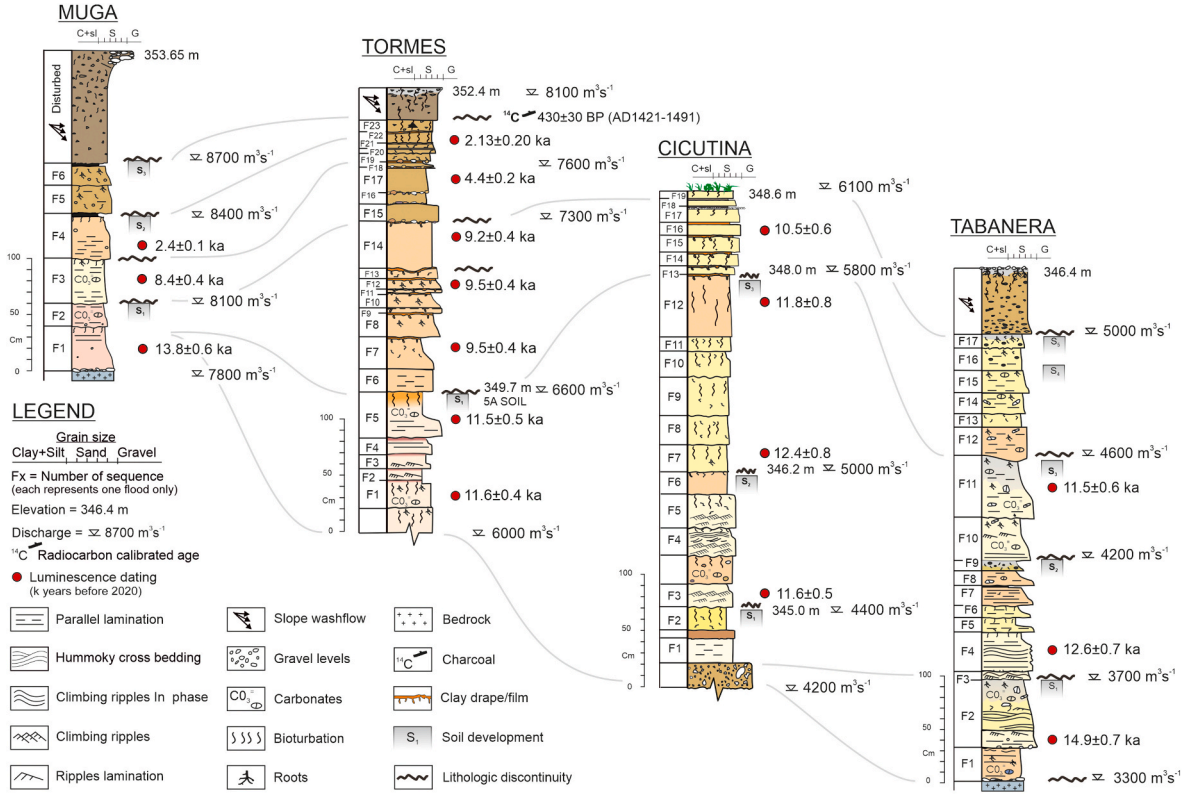

Fig. 5. Stratigraphic profiles with OSL ages, estimated peak discharges, and proposed stratigraphic correlations for the studied sections at the Duero-Tormes confluence. Site labels refer to locations in Figs. 3 and 4a. Altitudes of profile tops of described sections were determined from differential GPS survey and are in meters above sea level. Discharge values refer to the indicated flow stage computed by hydraulic modelling. OSL dates in ka before 2020. Note that in the Cicutina profile unit F3 was OSL dated to 11.6 ka, stratigraphically below units F7 and F12 dated to 12.4 ka and 11.8 ka, suggesting incomplete bleaching. These samples were laterally correlated with the central part of the Tabanera profile dated between 12.6 ka and 11.5 ka, which is stratigraphically consistent and within the same time frame as the Cicutina datings.

and consist of dark brown fine to very fine massive sand with increasing bioturbation towards the upper units (Fig. 4c and 5). The beds are separated by coarse sand and granules grains derived from the neighbouring hillside and the upper four units are overprinted by edaphic alteration. Flood beds To-17 and To-22 were OSL dated to 4.4 ± 0.2 ka and 2.1 ± 0.2 ka, respectively. In the uppermost flood bed, a charcoal chunk gave a radiocarbon age of CE1421-1491. The Tormes profile is capped by slope wash material that interrupted the deposition of younger flood units at this site.

The highest flood bench (Muga profile) contains at least six flood beds in four sets separated by unconformities and buried soils (Fig. 5). The flood beds are 30–40 cm thick, and consist of very hard, fine to very fine, massive sand with a high degree of edaphic alteration. Flood layers Mu-01, Mu-03 and Mu-04 were OSL dated to 13.8 ± 0.6 ka, 8.4 ± 0.4 ka and 2.4 ± 0.1 ka, respectively. The stratigraphy and geochronology therefore indicate a hiatus in flood deposition at this or higher levels, probably of several millennia between flood beds.

The Fox profile is located ~4 km downstream of the Duero-Tormes junction, at the left margin of the Duero River gorge, in a tributary mouth (Fig. 6a and b). The SWDs outcrop is 2.8 m thick and contains at least six flood beds that overlie a slope wash deposit of granules with a coarse sand matrix (Fig. 6e). The flood beds, 20–60 cm thick, consist of light brown fine sand, with massive to parallel lamination, and diffuse to clear contacts marked by pebble lines and textural changes. The flood layers have developed edaphic features and bioturbation. The lower flood layer (Fo-01) was OSL-dated to 10.3 ± 0.7 ka and the uppermost flood unit was OSL-dated to 2.9 ± 0.2 ka (Fig. 6e). This flood stack is overlain by a 35 cm thick, highly bioturbated colluvial deposit composed of dark brown, fine to coarse sand with occasional gravel clasts.

Downstream of the Duero-Tormes confluence, on the right margin (Portugal), a valley embayment contains three sand benches, at elevations of 21.63 m (Teso-1), 25.55 m (Enebro) and 29 m (Teso-2) above the river water level (Fig. 6a). The highest sediments (Teso-2) consist of a single 15 cm thick flood bed of fine to very fine sand bounded by two colluvial units with well-developed edaphic features in their upper parts

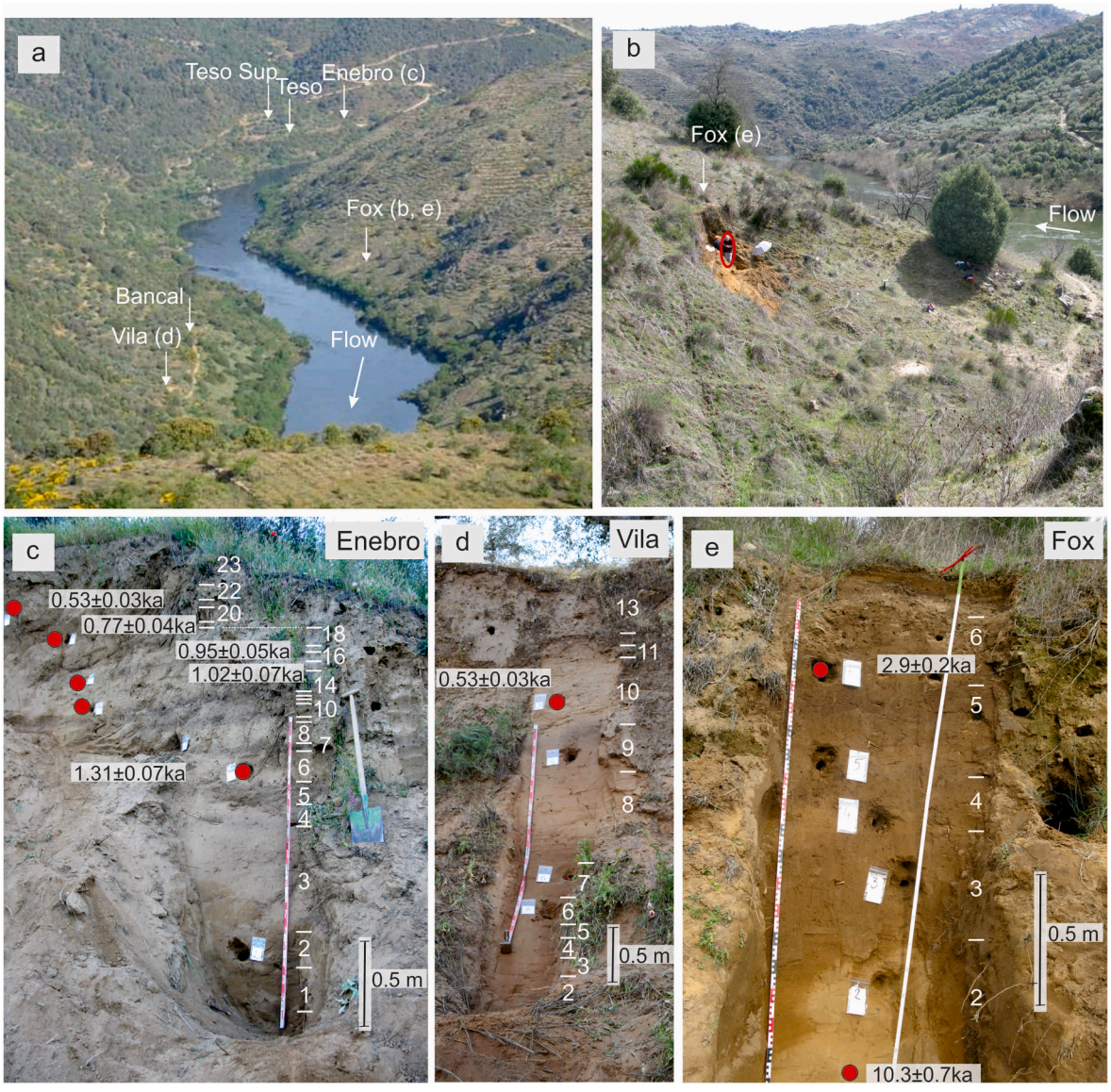

Fig. 6. Photographs from the lower Bemposta reach. a) Upstream view of the Duero River valley and location of the studied sections. Letters in brackets refer to detailed views in b, c, d, and e. b) Side view of the Fox section at a gully confluence. A person is marked with a red ellipse for scale. c) View of the Enebro profile showing light brown flood sand units overlain by distinct dark incipient soils (A horizons). Selected OSL dates (years before 2020) are shown. d) The Vila profile with a 0.5 m thick dark buried paleosol (above the second upper label) showing a break in deposition. The upper flood sequence (three flood beds) post-dates the last five centuries. e) Fine to very fine sand units in the Fox profile showing at least six flood beds with OSL dates bracketing the flood deposition period at this site.

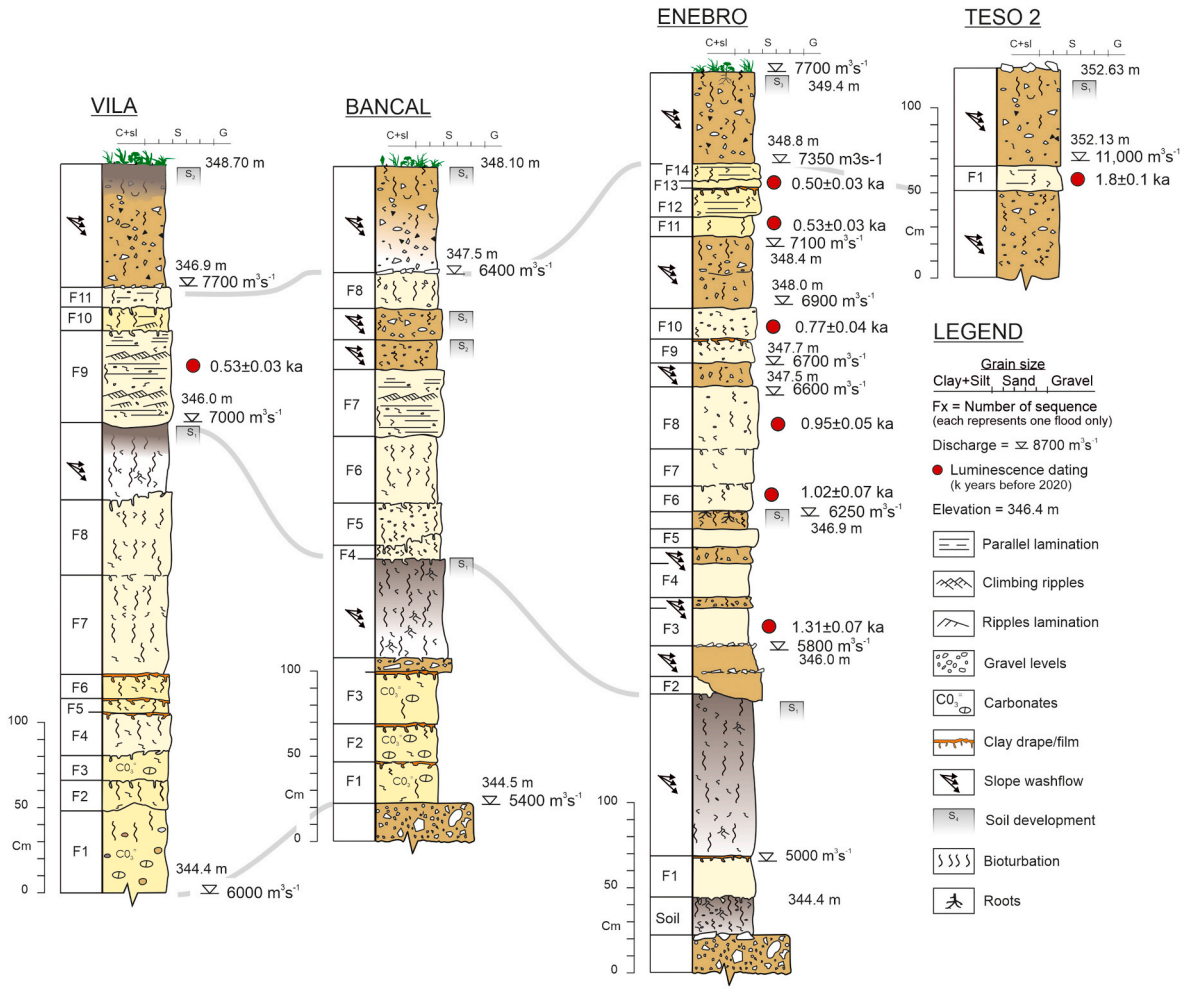

Fig. 7. Stratigraphic profiles with OSL ages, estimated peak discharges and proposed correlations in the lower Bemposta sites. Site labels refer to locations in Figs. 3 and 6a. Altitudes of tops of described sections were determined from differential GPS survey and are in metres above sea level. Discharge values refer to the indicated flow stage computed by hydraulic modelling. OSL dates in ka before 2020.

(Fig. 7). This unit, Te2-01, has been dated by OSL to 1.8 ± 0.1 ka. Near to this outcrop, the Enebro profile (5 m thick) preserves the most complete flood record of the last millennium (Fig. 6c and 7). The profile contains basal gravels capped by a buried paleosol (A horizon) overlain by a basal flood bed of unknown age (En-01). Overlying this flood bed is a ~1 m thick colluvium accumulated with a well-developed soil, probably representing a long period with a lack of flood bed deposition (Fig. 7). A second flood set consists of four flood beds (En-02 to En-05), 20–25 cm thick, light brown, very fine sand to silt, separated by clear contacts marked by angular stone lines and granules deposited from slope wash. The second flood unit (En-03) was OSL dated to 1.31 ± 0.07 ka. This flood set is capped by a colluvial unit overlain by dark brown soil (Fig. 6c). Above the buried soil, a third set consists of five flood beds (En-06 to En-10), 15–45 cm thick, of graded light brown fine to very fine sand, and conformable contacts eventually marked by thin granule lines. The basal, middle and upper units were OSL dated to 1.02 ± 0.07 ka, 0.95 ± 0.05 ka, and 0.77 ± 0.04 ka, respectively. The upper flood stack is overlying a 45 cm thick colluvium suggesting a further period of flood quiescence or dominance of slope processes. This upper set consists of four flood units (En-11 to En-14), 10–15 cm thick, composed of fine to very fine sand with parallel lamination, separated by diffuse and conformable contacts with root cast marks. The three lower flood beds are constrained by two OSL ages of 0.53 ± 0.03 ka, 0.50 ± 0.03 ka, while the uppermost bed post-dates the latter age (Fig. 7).

Downstream along the same right valley margin, the Teso (Te), Bancal (Ba) and Vila (Vi) profiles (Figs. 3 and 6a) show a multiple flood bed stratigraphy separated by colluvial units similar to the Enebro profile. In the Vila profile the upper stack comprises four flood units made of light brown fine sand, with current ripples, overlying a dark grey agricultural soil that is ubiquitous in the right Duero valley (Fig. 7). The basal flood unit overlying the soil was OSL dated to 0.53 ± 0.03 ka, a date similar to the upper Enebro flood set.

In the undated Teso profile, the lower stack comprises three flood units (Te-01 to Te-03) made of fine sand with interbedded reddish laminae of very fine sand to silt, with the upper unit being truncated by an erosive infilled rill contact. Overlying an unconformity, we identified three flood beds (Te-04 to Te-06) composed of fine sand, highly bioturbated and capped by a dark soil horizon with similar characteristics to the uppermost Bancal-Vila Enebro agricultural soil surface. The upper set above the agricultural soil is composed of at least five flood beds 15–25 cm thick and, unlike the rest of the SWD outcrops, it is not capped by slope wash or anthropogenic soils. This upper flood cluster likely is deposited by more recent flood events (probably within the last 400 years), although unfortunately no date are available for this upper flood stack.

4.1.2. *Saucelle reach*

The Saucelle reach is located ~500 m downstream of the Duero-Huebra confluence, between the municipalities of Saucelle (Spain) and Freixo (Portugal). The paleoflood depositional environment covers a

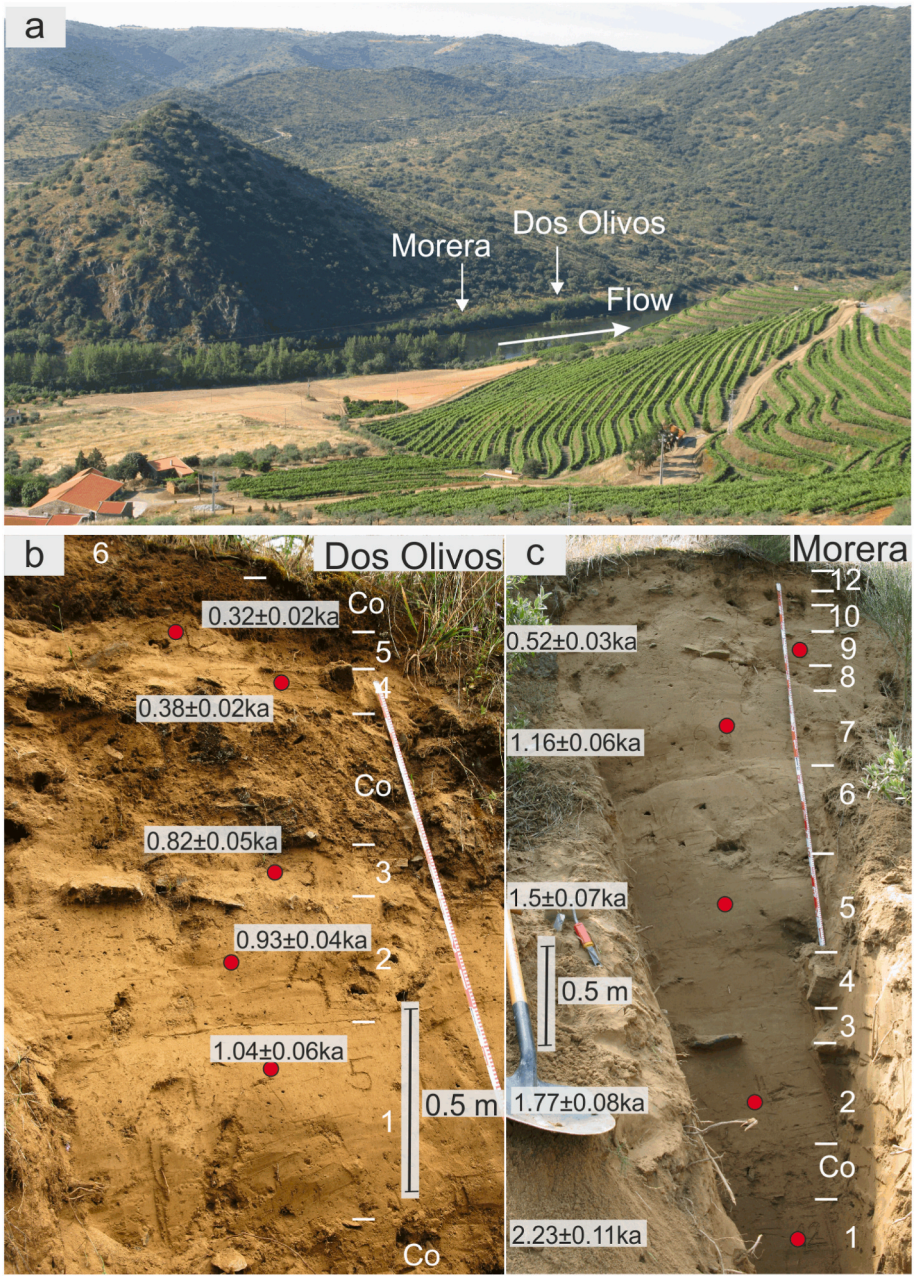

Fig. 8. Photographs from the Saucelle study reach. a) Downstream view of the Duero valley at the Saucelle reach with a flood bench formed on the lee side of a bedrock hill with the two SWD stratigraphic profiles - Dos Olivos and Morera. b) Dos Olivos profile, showing at least six flood beds with intercalated stone layers and colluvium (Co). c) Sequence of 12 flood beds with some contacts marked by stone lines and colluvium in the Morera profile. Selected OSL dates are shown.

canyon expansion about 1.3 km long and 200 m wide (Fig. 8a). The paleoflood deposits are preserved in a ca. 1 km long and 15.5 m high (a.r.l.) bench located on the lee side of a rock protrusion on the Spanish margin (Fig. 8a). The bench scarp shows multiple flood units, eventually intercalated with slope deposits. Two trenches, separated by about 20 m, were cut into this bench, named the Dos Olivos (DOL) and Morera (MOR) profiles. Profile DOL is 2.5 m thick and is composed of brown to yellow fine to medium sand units, with well-marked contacts, diffuse lamination to massive structure, with intercalation of slope deposits and stone lines along the palaeoflood unit contacts (Fig. 8b). The profile shows at least five flood units within three clusters separated by colluvial beds. A total of five OSL samples were collected from the site (Table 1). The lowermost flood beds (1–3) were constrained by OSL ages of 1.04 ± 0.06 ka, the middle set (units 4–5) were dated to 0.38 ± 0.02 ka and 0.32 ± 0.02 ka respectively, while the upper bed post-dates the latter age.

The Morera profile is 3.2 m thick and comprises 12 flood units separated by diffuse to well-marked contacts (stone lines; Fig. 8c). The lower flood units (1–7) are thicker (average of 35–40 cm) than the upper units (typical average thickness of 10–15 cm). Five OSL samples were dated between units 1 to 9 with ages ranging from 2.23 ± 0.11 ka to 0.52 ± 0.03 ka, while the upper three undated units correspond to historical floods.

4.2. *Hydraulic modelling and discharge estimation*

Hydraulic flood modelling was carried out along the Bemposta reach because it contains the most complete paleoflood record, allowing a long-term comparison of palaeoflood magnitudes over the last 15 ka. The conservative discharge estimates assume that the top elevation of a

flood unit was close to the peak stage of the flood event. The local geomorphological setting along the Duero study reach dictates the sedimentation and preservation of the flood sequences as well as the flood bed elevation, which ultimately provides the flood stage/peak discharge relationships (Fig. 9).

The large accommodation space at the Duero-Tormes confluence allowed the deposition of nearly 13 m thickness of flood sediments, considering the progressive accumulation in the Borbon (16.12 m a.r.l.), Tabanera (18.44 m a.r.l.), Citutina (20.75 m a.r.l.), Tormes (23.25 m a.r.l.) and Muga (26.5 m a.r.l.) profiles. At the Duero-Tormes confluence, the maximum flood magnitude was constrained by a range of discharges of 7800–8700 m^3/s of the flood units in the Muga profile, dated between 13.8 ± 0.6 ka and 2.4 ± 0.1 ka, although at least two flood units are likely to have been deposited in the last 2 ka. The Muga profile is capped by disturbed material from road works, so more recent flood evidence is missing at this site. The most complete temporal flood stack was found in the Tormes profile, with 23 flood beds deposited between 11.6 ± 0.4 ka to 0.5 ka and with minimum discharges from 6000 to 8100 m^3/s. The progressive thinning of flood beds in the upper Tormes profile suggests a deposition just below of the maximum flood level over the last 2 ka (Fig. 5). This profile is covered by slope deposits that contain a matrix of flood sand, meaning likely removal of flood units post-dating ~1500 CE (430 ± 30 C^{14} yr BP).

The range of minimum discharges required to overflow the flood bench on the Tabanera and Cicutina profiles, deposited between 14.9 ± 07 ka to 10.5 ± 0.6 ka, was between 3300 and 5000 m^3/s and 4200–6100 m^3/s, respectively (Fig. 5). In this bench, the Tabanera profile is covered by colluvium, indicating likely erosion of the uppermost flood sequences. In the Cicutina profile, the upper seven flood units dated to ~10.5 ± 0.6 ka are thinning upwards, probably because the palaeostage evidence relates closely to the maximum flood stage. Palaeoflood evidence for large flood events post-dating 10.5 ka is found on the Tormes and Muga profiles, at higher elevation benches and closer to the valley side, with modelled discharges exceeding 6600 m^3/s. This stratigraphic hiatus at the Cicutina-Tabanera bench indicates that during extreme floods, eddy currents are displaced towards the valley margins, creating a flood record that is sensitive to variations in flood stage and magnitude. The decreasing number of flood beds during the Middle and Late Holocene indicates a limited accommodation space at the Duero-Tormes confluence, but also a decrease in peak discharges that has only been reversed in the last two millennia. Historic to modern flood deposition occurs on the lowest bench at 16.12 m a.r.l. (Borbon profile) with modelled minimum discharges of 3600 m^3/s. This lower flood bench was last inundated during the 2001 flood with a discharge of 3854 m^3/s.

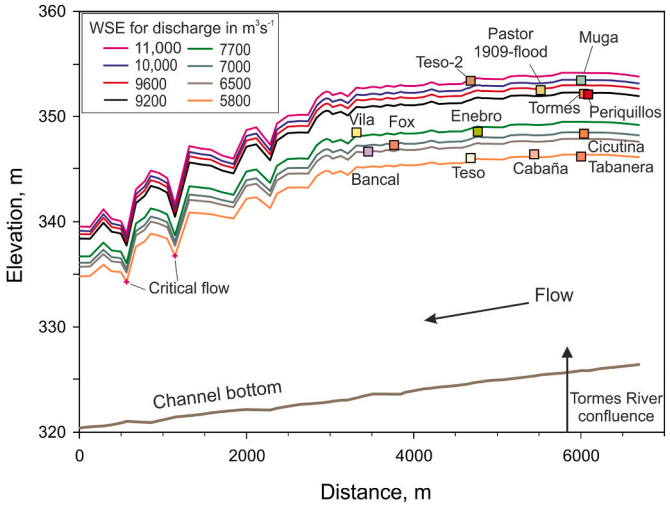

Fig. 9. Distribution of flood sediment sites and calculated water surface elevation (WSE) profiles for selected discharges along the Bemposta reach. The profile location is indicated in Fig. 3.

Evidence of the largest floods of the last two millennia is found on the right margin downstream of the Duero-Tormes confluence (Fig. 6a). The Enebro profile (24 m a.r.l.) was deposited from 1.31 ± 0.07 ka to 0.50 ± 0.03 ka with minimum discharges of 5000–7200 m^3/s and 4500–5900 m^3/s, respectively. In the Teso-2 profile, an isolated flood bed dated to 1.8 ± 0.1 ka, provided a modelled minimum discharge of 11,000 m^3/s required to deposit this sediment located 28 m above the river level. In the same valley expansion, the Teso-1 profile provided a modelled discharge of 5900 m^3/s, with no dated flood beds. Downstream, the Vila and Bancal profiles were associated with modelled discharges of 5400–6400 m^3/s and 6000–7700 m^3/s, respectively. These profiles show a similar stratigraphy to the Enebro site, although only the upper flood cluster at the Vila profile dated to 0.53 ± 0.03 ka with a minimum discharge of 7000–7700 m^3/s was required to overtop these sediments.

5. Discussion

5.1. Implication of channel bed incision for discharge estimations

The hydraulic modelling relies on the assumption of stable river geometry, meaning that the present topography and mapped landforms have not changed significantly through time. The absence of alluvial gravel terraces along the study reach indicates that there were likely no significant episodes of aggradation, at least during the Late Quaternary. However, it is important to note that the assumption of riverbed stability requires further consideration, especially in light of the average incision rates reported, such as 1.4 m/ka in the mid and lower Douro since the Late Pleistocene (Cunha et al., 2019) and 2–3 m/ka in the Duero canyon over the last ~100 ka (Antón et al., 2012). These incision values should be considered as long-term average rates, implying that specific reaches may have experienced higher or lower incision rates. In the Duero canyon, several knickpoints have been identified, often associated with lithological changes or tectonic structures (Struth et al., 2019). This suggests a spatial and temporal variability in migration and incision rates during the Late Quaternary. Struth et al. (2019) estimate an average migration rate of 0.02 m/yr for knickpoints in the Duero canyon, reflecting the low erodibility of the granitic bedrock.

As illustrated in Fig. 9, the water surface profiles reveal distinct characteristics along the lower 3 km segment, featuring steeper gradients and changes in the water surface slope. This contrasts with the relatively consistent and moderate slope observed in the upper 4-km segment. These variations in water surface slope correspond to a knickzone encompassing at least two knickpoints (see critical flow points in Fig. 9), which have been identified through aerial photographs and topographic maps. The morphological characteristics of these knickpoints include a stepped channel bed within a narrow valley section, followed by a semicircular widening of the channel downstream, likely resulting from flow eddies at the point where the channel slope changes. These knickpoints serve as indicators of active bed incision in river reaches with high energy expenditure, particularly during extreme floods. Note that during the Late Pleistocene and Early Holocene, these knickpoints were likely positioned further downstream, migrating upstream from sections with lithological changes or tectonic structures. In the upper 4-km segment (Fig. 9), the slope profile observed exhibits a consistent water surface slope without significant channel slope interruptions, indicating relative stability in the channel bed. However, two strath surfaces, of unknown age, have been identified at elevations of +2 m and +4 m above the river's thalweg, representing former channel bed levels. Assuming a Late Pleistocene to Holocene age for these levels, the uncertainty in our palaeoflood discharge estimates ranges from 115 to 350 m^3/s. This introduces an overestimation error of only 2–6% for the smallest palaeoflood (5800 m^3/s).

Larsen and Lamb (2016) argue that bedrock canyons adjust their geometry to a critical shear stress by progressively downcutting at

similar rates across both the lengths and widths of the channel bed. The threshold shear stress required to initiate erosion in bedrock canyons may vary depending on the mechanisms of bedrock erosion (e.g., plucking, flow abrasion, solution, cavitation; Whipple et al., 2000). For instance, Larsen and Lamb (2016) estimated a shear stress level exceeding 750 Pa as necessary for adjusting the bedrock canyon geometry during the Missoula floods, while Ortega-Becerril and Garrote (2023) associated the onset of lateral pothole erosion in modern Spanish rivers with a shear stress exceeding 580 Pa. These shear stress thresholds are typically reached during extreme floods, suggesting that low-flow conditions are insufficient to induce significant morphological changes. Our hydraulic model demonstrates that at cross-sections linked to knickpoints, channel shear stress fluctuates within the range of 400–500 Pa for discharges of 5800 and 11,000 m^3/s. In contrast, in the upper 4-km segment encompassing our stratigraphic sites, shear stress ranges between 30 and 70 Pa, respectively. Consequently, as the gradient and topography decrease, the effect of floods in channel erosion diminishes, while significant incision may take place in segments with changes in hydraulic geometry (e.g., bed steps, narrow valley sections). This implies that the incision of the strath surface in the upper segment (~4 m above the current riverbed) was mainly driven by geomorphologically effective events, specifically the 62 palaeofloods recorder in the stratigraphy. Long-term channel incision, therefore, follows a cyclical pattern, primarily concentrated during episodes of large floods, which in our case occurred during the ten flood clusters spanning 2350-years during the Holocene.

Consequently, both field evidence and hydraulic modelling results indicate that the present valley geometry provides a suitable basis for estimating palaeoflood discharges during the Late Pleistocene and Holocene. This analysis is further supported by the absence of a systematic bias toward higher discharges in modern times, as one might anticipate in cases of substantial channel bed erosion.

5.2. Duero River composite flood record

This section summarises the palaeoflood timing and magnitude compiled from the multiple stratigraphic profiles mainly from the Bemposta reach, complemented by flood chronologies from the Saucelle reach. Flood records older than 2 ka were assembled from the Tabanera, Cicutina, Tormes and Muga profiles, while events younger than 2 ka were collated from Enebro, Bancal and Teso profiles. We identify at least 62 flood events clustered in ten flood-rich periods (Fig. 10a). Each flood cluster includes dated and undated flood beds but the cluster time span is constrained by OSL dated units. In the flood clusters, the undated flood bed(s) have been assigned an interpolated age(s) at regular time intervals for representation purposes. The modelled minimum flood discharges within each flood cluster may contain information from several profiles. For example, in a cluster of ten flood beds postdating 11.6 ± 0.5 ka in the Cicutina profile with discharges above 4400 m^3/s, at least five floods exceeded 6000 m^3/s, which are also recorded in the basal sequence of the Tormes profile (dated to 11.6 ± 0.4 ka). Hence, we considered the possibility that some floods might be recorded in different stratigraphic profiles and therefore we included a conservative number of floods in the composite record.

The flood record for the last 2 ka is mainly derived from the Enebro profile (Bemposta reach). There are a number of undated flood units on the Enebro, Bancal and Vila profiles that are older than 1.31 ka that most likely occurred between 2 and 1.3 ka. In the Saucelle reach, a cluster of five flood beds at the Morera profile (Mo-02 to Mo-05) were deposited within the age range of 1.77 ka to 1.5 ka. We infer that their discharges were of the order of the floods preserved at the base of the Bancal-Vila profiles prior 1.3 ka.

The youngest flood beds in the Bemposta reach were dated to ~0.53–0.50 ka (Enebro and Vila profiles) and CE 1421–1491 (To-23), whereas in the Saucelle reach the youngest flood bed was dated to 0.32 ± 0.2 ka (Do-05). This latter flood bed in the Saucelle reach is close in time to the CE 1739 flood, the largest in the last 300 years according to the historical flood marks at Régua (Silva and Oliveira, 2002). Other undated flood beds in the upper section of stratigraphic profiles of Vila (Vi-10 or Vi-11), Enebro (En-14), Tormes (To-23) and Muga (Mu-05-Mu-06) were probably exceeded by the 1739 flood ($Q > 8700$ m^3/s). Unfortunately, most of the above mentioned flood beds are undated.

The largest floods over the last two centuries occurred in 1860 and 1909, with documentary evidence of flood levels recorded at various points along the international Duero/Douro River. In the Bemposta reach, the 1909 flood level is well documented on the topographic map of the dam project. Some 40 km downstream, near the village of Mazouco (Portugal), the Saucelle dam project provides a detailed sketch of a farm building showing that the 1860 flood level was ~0.2 m lower than the 1909 flood. Next to the Aldeadavila dam wall, the 1860 flood stage was 0.6 m lower than the 1909 flood, according to several marks made on buildings and carved into rocks by local people. In the Bemposta reach, a field inspection of the mapped 1909 flood level revealed an abandoned small shepherd's hut. A 20 cm pit dug into the ground of the hut exposed at least two flood units made of light brown fine sand with ripple marks. We infer that these flood beds were most likely deposited by the 1909-flood (marked in the dam project report), which most likely overlay the 1860 flood bed.

5.3. Flood variability in relation to regional paleo-hydroclimatic records

In this section, the 62 flood events, grouped into ten flood periods (FP1 to FP10; Fig. 10a), are compared with hydroclimatic records from terrestrial and marine proxies in NW Iberia (Fig. 10). The Holocene paleoclimate records include: (1) the reconstruction of the sea surface temperature (SST) of the Iberian marine margin (Fig. 10b, MD95-2040-125 km west of Porto; de Abreu et al., 2003) and MD03-2697 (Naughton et al., 2016); (2) the discharge of the Tera River into Lake Sanabria (Fig. 10c) inferred from geochemical proxies (Jambrina-Enríquez et al., 2014); and (3) water/sediment fluxes based on pollen and mineralogical analysis of sediment cores in the Douro estuary (Naughton et al., 2005; Rocha et al., 2002). The chronology and magnitude of the Duero floods were compared with existing palaeoflood records in the Tagus (Benito et al., 2003b) (Fig. 10d) and Guadiana (Ortega and Garzon, 2002), as well as with regional flood activity derived from metadata analysis of palaeoflood chronologies in Iberian rivers (Benito et al., 2015c).

5.3.1. Late Pleistocene-Early Holocene

The oldest flood evidence is found at the base of Tabanera (Ta-01 and 02) and Muga (Mu-01 and 02) in two sets (FP1a, 1b; Fig. 10a) spanning ages from 14.9 ± 0.7 to 13.5 ± 0.6 ka with associated minimum discharges ranging from 3700 m^3/s to 8100 m^3/s (Fig. 10e). Climatically, this period (FP1b) overlaps a warm and humid phase of the Bølling-Allerød interstadial (14.6–12.8 ka), which is characterized in Lake Sanabria (Fig. 10c) by a distinct deposition of organic silt, indicating an increase in lake bioproductivity (Jambrina-Enríquez et al., 2016). The Muga flood beds contain a well-developed paleosol with iron precipitate concretions, suggesting relatively wet climatic conditions, as well as a long period without flooding above a threshold of ~8100 m^3/s after 13.5 ka that likely lasted until 8.4 ± 0.4 ka. A second sequence of 11 flood beds, in two sets dated to ~12.6 ka (2 floods; FP2a) and ~11.5 ka (9 floods; FP2b), were inundated by floods exceeding 3800 m^3/s and 4575–6600 m^3/s, respectively (Fig. 10e). These flood periods coincide with the onset and end of the Younger Dryas period (YD; ~12.9 to 11.7 ka; Alley, 2000). The lack of large floods during most of the YD period is consistent with climate proxies indicating aridity during this cold episode (Morellón et al., 2009; Moreno et al., 2011; Muñoz Sobrino et al., 2001; Santos et al., 2000) and extremely dry YD winters in northern Iberia based on regional stalagmite records (Baldini et al., 2019). The lack of major floods during the YD is also reported for the Tagus River (Benito et al., 2003b). These palaeoflood records suggest a

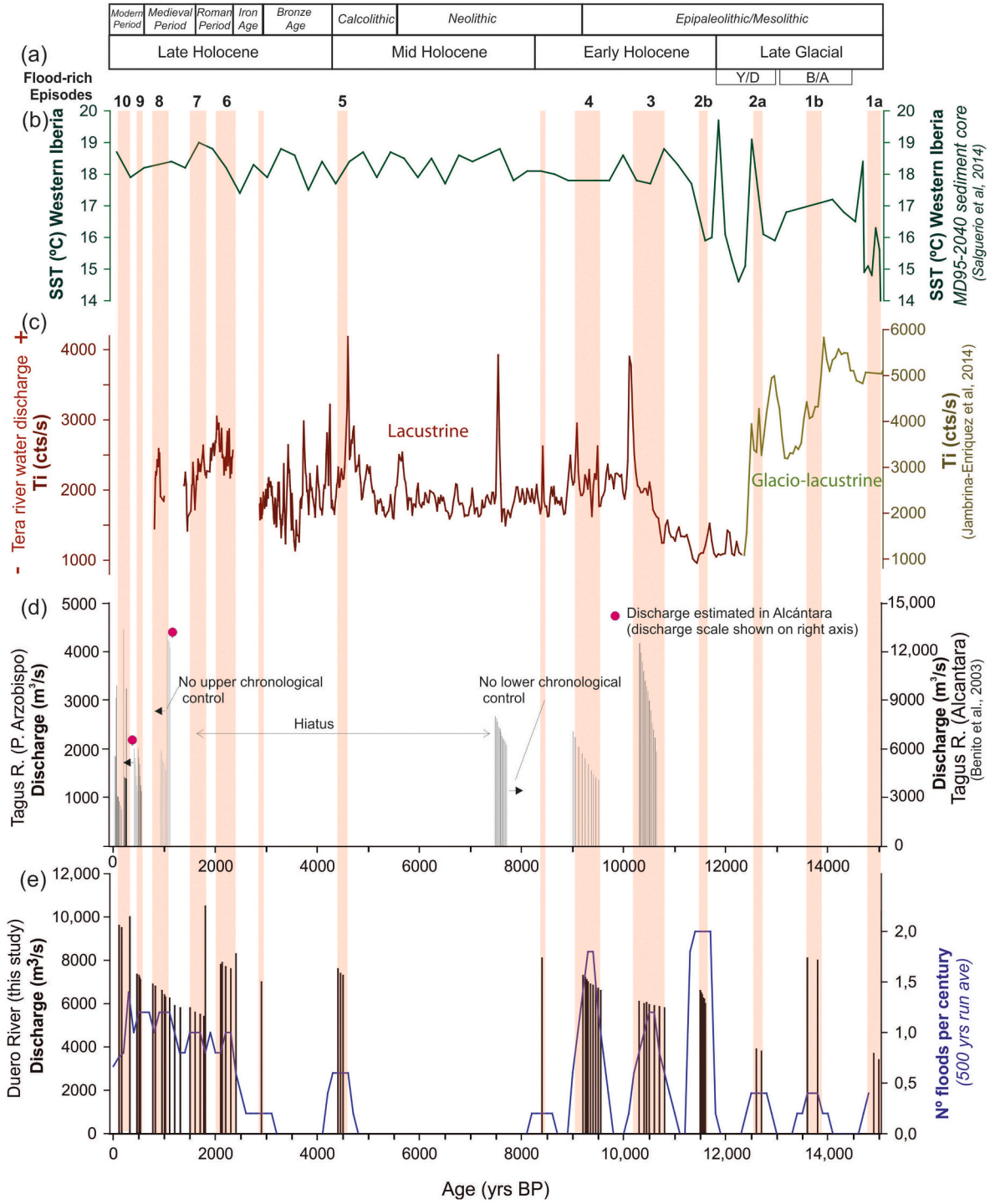

Fig. 10. Temporal distribution of hydroclimatic and marine records in the Iberian Atlantic region. (a) Flood episodes based on the Duero River record (this study). Vertical shaded bars with numbers indicate flood-rich episodes (>3 flood events), while the shaded bars without numbers indicate an isolated large flood within the time period. In other periods, floods were either below the discharge threshold or not recorded in the palaeoflood stratigraphy; (b) Reconstruction of the sea surface temperature (SST) of the Iberian marine margin from the core MD95-2040 (de Abreu et al., 2003); (c) Temporal distribution of geochemical content of the Ti (cts/s) from the Sanabria Lake core, interpreted as a proxy for the water discharge of the Tera River (Jambrina-Enríquez et al., 2014). Note that peaks of water discharge in the lake are visually correlated with high flood recurrence periods represented as number of floods per century; (d) Combined palaeoflood record of the Tagus River from Puente del Arzobispo (central Spain) and Alcántara (western Spain), each bar corresponds to a flood bed (Benito et al., 2003a,b); (e) Flood distribution and quantified discharges for the Duero River during the Late Pleistocene-Holocene (this study). The timing of undated floods was interpreted on the basis of their stratigraphic position, bracketed by dated flood beds. Legend: Y/D: Younger Dryas period; B/A: Bølling-Allerød interstadial.

decrease in the seasonal (winter-spring) persistence of cyclonic winter precipitation in western Iberia. Following the YD, a period of high flood frequency at ~11.5 ka (FP2b), has been documented, with thick SWD accumulations in the Cicutina and Tabanera profiles, suggesting a southward shift of the cyclonic circulation during the transition to the Holocene, prior to the 11.2 ka cooling event (Muñoz Sobrino et al., 2007, 2013). The upper surface of the ~11.5 ka flood sediments evolved into the formation of a Bt horizon (well developed on To-05 unit), which together with other pedogenetic features suggests a subsequent period of low flood frequency. Pollen records from lakes in NW Iberia show an increase in tree pollen taxa and higher lake levels centered around 11.8–11.5 ka (Muñoz Sobrino et al., 2007, 2013), interpreted as a regional expansion of woodland cover (Jambrina-Enríquez et al., 2014).

A later flood episode (10.8–10.3 ka) overlying the Cicutina and Tabanera profiles comprises at least seven floods (FP3) with minimum discharges of 5800–6100 m^3/s, probably represented at the Fox profile (Fo-01 to Fo-05) with discharges exceeding 6100–7000 m^3/s (Fig. 10e). These two sites record repeated floods with progressively higher discharges. This is because a higher stage is required to deposit a subsequent flood unit at a given location. However, the frequency of large floods in this flood episode is anomalously high and coincides with a similar flood episode in the Tagus River with at least 12 events dated to 10.5–10.1 ka BP (Fig. 10d). This FP3 cluster overlaps a period of high river sediment supply to the Douro estuary (Naughton et al., 2007; Rocha et al., 2005). Climatically, FP3 coincides with a trend to warmer SST conditions at the onset of the Holocene, as reflected in the Atlantic marine core (de Abreu et al., 2003; Fig. 10c). The regional evidence of an anomalous number of large floods in the Iberian Atlantic river basins (Tagus and Duero) is interpreted as an indication of a period of wet winter conditions occurred at this time, associated with a low-index zonal circulation over the Atlantic.

The next flood cluster FP4 with preserved geomorphic evidence is associated with eight to nine flood beds deposited at the Tormes profile (To-06 to To-13) at ~9.5–9.2 ka with discharges exceeding 6600–7300 m^3/s. These flood units are separated by clay laminae with a lack of erosional or edaphic processes interpreted as indicating relatively short intervals between flood units. A similar flood episode in the Tagus River (Fig. 10d) comprises ten flood beds made of fine sand to medium sand graded rhythmites dated to 9–9.5 ka BP (Benito et al., 2003b). Records from Lake Sanabria include coarse clastic layers at 10.1–8.4 ka BP associated with large flood events (Jambrina-Enríquez et al., 2014). Several lakes in the Iberian Peninsula register high stands and forest development at 10–8 ka (e.g., Morellón et al., 2018), consistent with speleothem proxies indicating wet conditions at 11.7–8.5 ka (Moreno et al., 2017).

An OSL age of 8.4 ± 0.4 ka was obtained for a 0.5 m thick flood bed deposited in the Muga profile, over a well-developed Late Pleistocene soil, with a discharge exceeding 8250 m^3/s. This individual flood event is one of the largest on record, but it is not correlated with other regional flood clusters. Stalagmite isotope data from western Iberia indicate rapidly drying conditions centered around 8.4 ka BP (Thatcher et al., 2020), and several pollen and lake records indicate dry climatic conditions between 8.5 and 8.1 (Carrión, 2002; González-Sampériz et al., 2006; Jalut et al., 2000; Morellón et al., 2008). This evidence suggests that this single extreme flood event occurred in the context of a highly variable hydroclimate. The 8.4 ka flood bed contains edaphic features, including the formation of carbonate concretions, indicate of drier conditions.

5.3.2. Middle Holocene

The paleoflood stratigraphic hiatus at 8.4–4.4 ka is interpreted as a period without flooding above a threshold of ~6100 m^3/s necessary to inundate the Cicutina profile (Fig. 10e). The lack of stratigraphic evidence therefore is explained by the high discharge threshold required to deposit the subsequent flood-bed on the existing stratigraphic benches. In other Atlantic Iberian rivers, lower inset benches were formed in response to lower dominant flood discharges (Benito et al., 2015c). For instance, Tagus River floods dated to ~7.5 ka deposited a lower inset bench associated with a moderate to low magnitude discharge (2000–3000 m^3/s). Climatically, this flood-poor period overlaps with the Holocene Thermal Maximum (8.2–4.2 ka), which was characterized by warming of northwestern Europe that was balanced by cooling over southern Europe especially during the winter months (Davis et al., 2003). In NW Iberia carbonate isotopes record drier intervals alternating with wetter ones (Thatcher et al., 2020), as well as a change in rainfall seasonality with relatively drier winters between 7.5 and 4.6 ka (Baldini et al., 2019), interpreted as variable hydroclimatic conditions. At the Douro estuary, infill sediments showed an increased marine influence since 9.8 ka, with a marked intensification around 6 ka (Drago et al., 2006).

5.3.3. Late Holocene

After four millennia of quiescence, flood activity increased at ~4.4 ka (FP5) with deposition of three flood beds (To-15 to To-17) and minimum discharges of 7300–7600 m^3/s (Fig. 10e). Alluvial overbank deposition has been recorded in other Iberian catchments with hydrology controlled by the influence of Atlantic frontal systems, such as the Guadalete River (southern Spain) at 4.6–4.3 ka (Wolf and Faust, 2015; Wolf et al., 2014) and the lower Tagus River at 4.9–3.5 ka (Vis et al., 2010). Lake Sanabria recorded a sequence of frequent clastic laminae at 4.8–3.3 ka related to flood episodes followed by a second depositional phase at 3.3–1.5 ka with fewer discrete clastic facies (Fig. 10c) (Jambrina-Enríquez et al., 2014). This ~4.4 ka flood cluster coincides with a shift towards more humid conditions during the Late Holocene (Magny et al., 2013; Vannière et al., 2013) and the onset of episodes with a predominant negative NAO-mode due to a southward migration of the zonal circulation (Olsen et al., 2012).

The uppermost flood bed of the Fox profile (Fo-06) was dated to ~2.9 ka with a minimum discharge of 7000 m^3/s. It is unclear whether this event was isolated or formed a flood episode with three undated flood beds (Fo-3 to Fo-5), all with similar textural characteristics and with evidence for edaphic features at their contacts. In the Jarama River, a major tributary of the Tagus River, a period of alluvial accumulation has been dated to 2.8 ka (Wolf et al., 2013), while other proxy records show a transition from arid to humid conditions at ~2.9 ka in eastern Spain (Roca and Juliá, 1997). This flood chronology is coetaneous with a decline in solar activity at ~2.8 ka (Van Geel et al., 1998), which led to widespread cooling in the North Atlantic and increased humidity (Martin-Puertas et al., 2012). This flood bed(s) overlaps a flood-rich episode identified in west-central Europe (Benito et al., 2015b; Macklin et al., 2006) and the northwestern Mediterranean region (Benito et al., 2015c).

A series of five flood beds (FP6) preserved in the Tormes profile (To-18 to To-22) were constrained by an OSL age of 2.4 ± 0.1 ka (Mu-04) at the bottom and 2.1 ± 0.2 ka (To-22) at the top. Their contacts, marked by stone layers and colluvium, indicate a period of environmental instability due to human and natural stressors. These floods are associated with a lower minimum discharge of 7600–7900 m^3/s, and at least one flood exceeding 8300 m^3/s (Mu-04). This FP6 (2.4–2.1 ka) overlaps with an episode of flood activity identified in western and eastern Iberia at 2.8–2.2 ka (Benito et al., 2015c).

The largest flood on record (TS-01) was dated at 1.8 ± 0.1 ka with a modelled discharge of >10,500 m^3/s (Fig. 10e). Although this flood bed was found at a much higher elevation than other nearby profiles (Enebro and Teso), its chronology coincides with the onset of a flood cluster (FP7) composed of five flood beds described in the Morera profile (Mo-02 to Mo-05) and dated between 1.77 ± 0.08 and 1.5 ± 0.07 ka. We infer that these floods are probably those preserved in the Bancal (Ba-01 to Ba-03) and Enebro (En-02) profiles, with a minimum discharge of 5400–5800 m^3/s.

The second half of the first millennium comprises at least two flood beds preserved in the Enebro profile (En-03 to En-05), the lowest of

which is dated at 1.31 ± 0.07 ka, with discharges of 5800–6250 m^3/s. These flood beds are intercalated with colluvium interpreted as an episode of scattered floods alternating with slope degradation within a general trend towards a drier climate. This period overlaps with the end of the Dark Ages Cold Period (DACP; CE 460–775), a cold and wet episode in Europe (Helama et al., 2017), which experienced a progressive trend towards wetter conditions in northern Spain (Corella et al., 2013) and a reactivation of flood events recorded in Lake Arreo (Corella et al., 2021).

A sequence of three flood beds (En-06 to En-08) dated between 1.02 ± 0.07 and 0.95 ± 0.05 ka (FP8), with minimum discharges of 6100–6300 m^3/s, marks FP8 (Fig. 10e). These flood beds temporally coincide with the Medieval Climatic Anomaly (MCA; CE 900-1300). During the MCA the frequency and magnitude of floods in the Tagus River increased, as is evident by palaeoflood records (1.2–0.8 ka, Benito et al., 2003b) and documentary sources, namely between CE 1150 and 1200 (Benito et al., 2003a).

At the end of the MCA, two floods were recorded, dated at 0.82 ± 0.05 ka (En-09) and 0.77 ± 0.04 ka (En-10), with a minimum flood discharge of 6300 m^3/s. The second date is close in time to the largest flood documented in the Duero River at Zamora in Dec 1258 (Benito et al., 2021). Both the palaeoflood and the historical record show a period of flood quiescence between 0.77 ka and 0.53 ka. Interestingly, the Tagus palaeoflood record, like other Iberian lake records (Corella et al., 2016), showed a period of low flood frequency between 0.80 ka and 0.56 ka, suggesting a decrease in flood-producing atmospheric conditions at the transition between the MCA and the Little Ice Age (LIE; CE 1300–1850).

The FP9 includes four flood beds in the Enebro and Vila profiles that, together with a flood bed age from the Dos Olivos profile, constrain this period to 0.53–0.46 ka. Flood discharges at this time exceeded 7200 m^3/s in the Enebro profile and 7700 m^3/s in the Vila profile. At least one of these floods is preserved in the upper sequence of the Tormes profile (To-23) dated to CE 1420–1490 with a minimum discharge of 8100 m^3/s. Documentary data from Zamora include three floods that overlap the palaeoflood chronology and exceeded 2500 m^3/s, occurring in CE 1485, 1586, 1597.

The post 1600s flood record is not well constrained by the stratigraphic and chronological data. The upper flood beds of the Enebro-Bancal-Vila profiles are sealed by ~1 m of colluvium from agricultural terraces with poor preservation of flood layers over the last 400 years. Instead, flood beds with modelled discharges between 4000 and 5000 m^3/s were recorded in the Borbon and Teso profiles, unfortunately without age dating. In the undated Teso profile, the most recent flood stack contains five flood beds with a minimum flood discharge of 5300 m^3/s. This stratigraphic configuration is similar to the Dos Olivos profile (Fig. 8b) with an upper sequence of four flood beds, the lowest of which was dated to 0.46 ± 0.03 ka. The overlying bed was dated to 0.32 ± 0.02 ka, within the age range of the 1739 flood, the largest recorded over the last 300 years according to the historical flood marks at Régua (Silva and Oliveira, 2002). We infer that the upper two flood beds in Dos Olivos may correlate with the two flood beds in the Pastor profile, which according to documentary data, were inundated during the 1860 and 1909 floods (FP10, 0.3–0.11ka; Fig. 10e). The minimum discharges of these two floods in our study reach are 9500 m^3/s and 9600 m^3/s, respectively. According to Silva and Oliveira (2002), the discharges of the 1739, 1860 and 1909 floods in Régua (Fig. 1b) were estimated as 18,000 m^3/s, 15,100 m^3/s and 16,700 m^3/s, respectively. These authors reported in Régua other two other large floods in 1788 (15,500 m^3/s) and 1823 (15,600 m^3/s), which were estimated at 2550 m^3/s and <1500 m^3/s in Zamora (Benito et al., 2021). In Vila Nova de Gaia (near Porto; Fig. 1b), these floods reached stages of 8.74 m and 8.34 m that are similar to 8.48 m for the 1966 flood measured in Miranda (Fig. 1c) with a discharge of 5872 m^3/s, below the minimum discharge required to left sedimentary evidence on the studied flood benches. During the second half of the 20th century the largest flood in Régua occurred in 1962 with an estimated discharge of 15,700 m^3/s, although in our study reach it was ~7700 m^3/s according to the gauged data at Puente del Pino and Miranda (Fig. 1b and c).

5.4. Atmospheric circulation and regional flooding

One of the major challenges of climate change science is to elucidate the effect of climate drivers on the temporal and spatial distribution of extreme floods at regional scale. This section provides an overview of the regional to hemispheric climate drivers that explain the centennial and multi-centennial flood variability of the Duero River. The Late Pleistocene-Holocene multi-centennial flood patterns are attributed to three main forcing mechanisms (Fig. 11): (1) long-term orbital-driven summer and winter insolation (Berger and Loutre, 1991) (Fig. 11a); (2) variations in solar activity amplified by meltwater pulses from continental ice sheets (Bond et al., 2001; Mayewski et al., 2004) and (3) the strength of the thermohaline circulation conditioned by changes in the subpolar gyre (SPG) or the subtropical gyre (STG) (Thornalley et al., 2009) and their feedbacks with the North Atlantic Oscillation (NAO) (Mayewski et al., 1997; Olsen et al., 2012).

The Late Pleistocene to Early Holocene transition was characterized by the absence of extreme floods in the Duero River coinciding with the dry/cold climate of the Younger Dryas (~12.9–11.7 ka). This cooling event resulted from a weakening of the Atlantic Meridional Overturning Circulation (AMOC; Bakke et al., 2009; McManus et al., 2004) with a shift of the Azores high pressure centre to lower latitudes, which hindered subtropical flow towards northern latitudes. The transition from the YD to the Early Holocene was marked by a sharp rise in lake levels in N-NW Iberia (Morellón et al., 2018), probably indicating a higher rate of winter precipitation and flooding, as also recorded by regional palaeohydrological proxies from stalagmites from northern Iberia (Baldini et al., 2019).

During the Early Holocene, flood-rich periods (ca. 11.5 ka, 10.8–10.3 ka, 9.5 ka) coincide with a broad millennial climate cycle that is consistent with the temporal cycles of meltwater pulses (11.4 ka, 10.4 ka and 9.4 ka; Fig. 11c), which induced variations in the ocean-ice-atmosphere mechanism (Bond et al., 2001). Periods of deglaciation in the North Atlantic most likely reflect the weakening of the subpolar gyre (SPG) circulation (Fig. 11d) as the North Atlantic Current (NAC), which is mainly fed by the subtropical gyre (STG), becomes warmer and saltier (Came et al., 2007; Hátún et al., 2005). This variability in oceanographic conditions has been accompanied by an atmospheric reorganisation (Repschläger et al., 2017; Thornalley et al., 2009) with a reactivation of northward heat transport from tropical and subtropical regions. We speculate that the Duero flood-rich periods provide evidence for intervals of enhanced moisture transport from the tropics. Indeed, the weakening of the SPG circulation is most likely to occur in conjunction with meltwater pulses (Fig. 11c and d) or with the meridional atmospheric circulation (Thornalley et al., 2009), as occurred in the 1960s when the Duero River recorded six exceptional floods (Fig. 12a). Bond et al. (2001) suggested that a 1500-year cycle of regional cooling, encompassing the variability in North Atlantic Deep Water formation, was amplified by solar activity (e.g., grand solar maxima). Temporal historical flood patterns in the Tagus River are linked to secular solar maximum activity through its control on the NAO, which influences precipitation variations in Iberia (Benito et al., 2003a; Vaquero, 2004).

The palaeoflood record of the Duero River shows the absence of major floods between 8.4 ka and 4.4 ka, coinciding with the Climatic Optimum (8–4 ka). During the Holocene Optimum, model simulations show tropical cooling due to reduced tropical winter (DJF) insolation (drop of ~ -20 Wm^{-2} compared to modern distribution) with an enhanced Azores high (Lohmann and Lorenz, 2000). This winter insolation contrasts with the intensified northern hemisphere summer insolation, representing the warmest climate in the last glacial cycle (Berger, 1978; Lohmann and Lorenz, 2000). Marine records show an enhanced subpolar gyre circulation during the Mid-Holocene

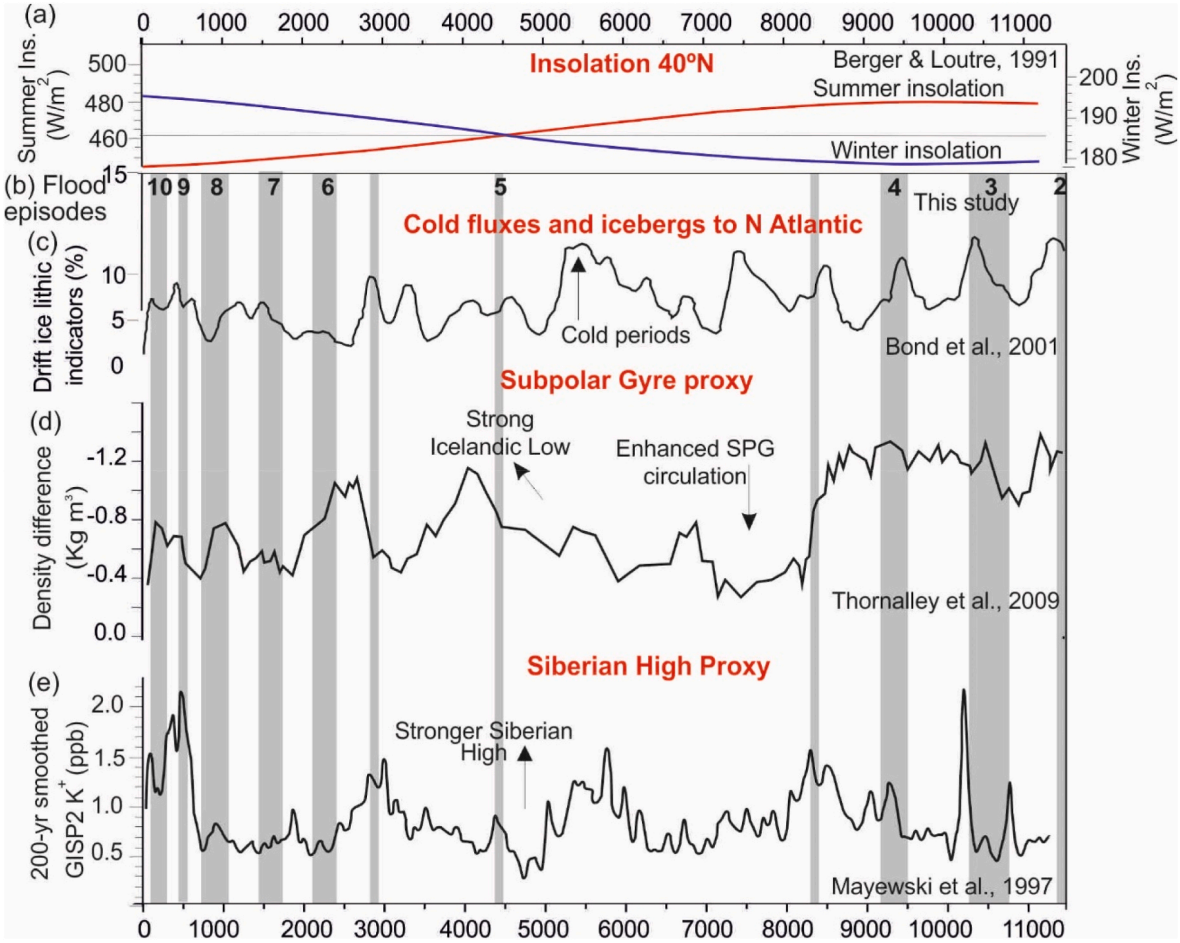

Fig. 11. Phases of enhanced flood activity of the Duero River (vertical grey shaded bands) related to palaeoclimate proxy records. (a) Summer and winter insolation curves at 40°N due to orbital parameters that show a decrease in summer insolation and an increase in winter insolation since the Early Holocene maximum around 10 ka (Berger and Loutre, 1991), affecting the seasonal distribution of temperature and the intensity of local seasons; (b) North Atlantic drift ice index (Bond et al., 2001). (c) Dynamics of the North Atlantic subpolar gyre (SPG) reconstructed from the marine water density difference between G. bulloides and G. inflata (Thornalley et al., 2009). (d) Gaussian smoothed (200 yr) potassium (ppb K^+) ion from the GISP2 ice core as proxy for the strength of the Siberian High (blocking conditions in the European region) (Mayewski et al., 1997).

(Thornalley et al., 2009; Fig. 11d), with a shift of winter cyclones towards high latitudes. Other geochemical proxies from the GISP2 ice core are consistent with high values of non-sea-salt calcium dust concentration (nss Ca^{++}), reflecting the strengthening of westerly winds from high latitudes (Mayewski et al., 1997). Both model and proxy observations are consistent with a climate scenario of reduced large floods (Fig. 12b), which does not imply that moderate to small magnitude floods could not have occurred.

During the Late Holocene (last 4 ka) proxy reconstructions show alternating periods of positive and negative NAO phases in the context of increasing winter solar insolation (Rimbu et al., 2003) (Fig. 11a). In the Duero River, flood-rich periods during the last 4.4 ka are consistent with the increase of decadal and multidecadal episodes with negative NAO modes (Fig. 12a). These atmospheric conditions with meridional flow are conditioned by atmospheric blocking situations (weak westerlies and strong Siberian High), which facilitate the southeasterly track of cyclones towards the Iberian Peninsula (Trigo et al., 2004b). Some flood episodes correspond to relatively cool temperatures (4.5–4.4 ka, 1.8–1.5 ka, 0.53–0.46 ka and 0.32–0.11 ka), but others overlap with warm conditions (2.4–2.1 ka and 1.1–0.8 ka) in southwestern Europe. This observation suggests that flood-generating processes in South Atlantic Europe were driven by other atmosphere-ocean coupling conditions rather than by temperature changes (warm-cold) alone. For instance, atmospheric blocking in the North Atlantic tends to promote the advection of moist air masses or Atmospheric Rivers from the warmer Caribbean Sea and the subtropical regions, producing widespread rainfall on low-to-mid latitudes of either side of the Atlantic (Häkkinen et al., 2011; Ballesteros-Cánovas et al., 2019).

In relation to the drivers, Barriopedro et al. (2008) describe that blocking persistence increases in the Atlantic basin during winters with low solar activity, being associated to negative NAO phase. A more spatially dependent response is found during winters with high solar radiation. In Europe, winter atmospheric blocking usually is induced by the intra-seasonal amplification of the Siberian High (SH) pressure cell over western Asia (Perşoiu et al., 2019). A proxy reconstruction of the SH (Mayewski et al., 1997) shows several strengthening periods (peaks) that overlap with episodes of flooding in the Duero River (Fig. 11e and 12a). As blocking episodes can persist for several weeks, they tend to produce significant precipitation and temperature anomalies.

5.5. *Current flood pattern in the context of centennial to millennial time*

On the centennial to millennial timescale, flood magnitudes have decreased during the 20th century under climate change conditions (Fig. 2a). The largest floods on record occurred in 1962 and 1939 with estimated discharges at the Bemposta reach of 7300 m^3/s and ~7000 m^3/s, respectively. Flood peaks have decreased even more in the last 40 years, with maximum annual discharges in the International Duero

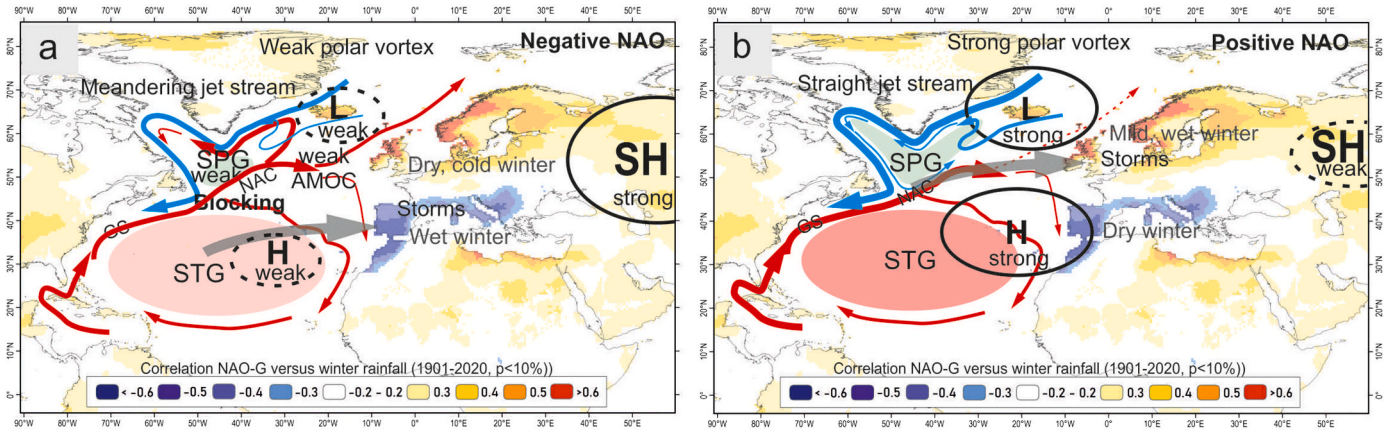

Fig. 12. Main components of the atmospheric and ocean circulation during periods of negative (a) positive (b) and NAO phases. The yellow and blue background on continental regions shows the correlation (r^2) between NAO-Gibraltar index and the precipitation from CRU TS4.06 precipitation dataset (wrt: 1901–2020, $p < 10\%$). Correlations are averaged-computed for November–March in order to match with the main flood season in the Duero basin. Atmospheric circulation centers of actions in the North Atlantic Basin and Europe (Icelandic and Azores pressure cells, and Siberian High-SH) are shown in black lines. Continuous lines show strong conditions of Low and High pressure centers and dashed lines indicates weak pressure conditions. Grey thick transparent arrow shows general vector of the vertically integrated moisture transport during negative NAO index (a) and positive NAO index (b) after Hurrell (1995) and Hurrell et al. (2003). Modern surface water hydrography of the North Atlantic currents are modified from Schott et al. (2004) and Repschläger et al. (2017). Warm surface currents are shown by red arrows, and cold currents are shown by blue arrows. Line thickness reflects relative flow rate. Legend: G.S., Gulf; N.A.C., North Atlantic Current; AMOC, Atlantic Meridional Overturning Circulation; SPG, North Atlantic Subpolar Gyre; STG, Subtropical Gyre.

being less than 5000 m^3/s. Although this decline in peak discharge may reflect an increase in flood regulation by dams, the limited storage capacity of dams on the International Duero/Douro River alone does not explain this significant reduction in flood magnitude. This decrease in peak flows coincides with a period of a dominant positive winter NAO phase since the 1980s (Rodrigo, 2021; Trigo and Gimeno, 2009) and a weakening of the Siberian High (Gillett et al., 2003b; Trenberth et al., 2007).

Most climate models simulate a shift to a positive winter NAO index associated with increasing concentrations of greenhouse gases, whereas the natural forcing is unlikely to be a significant component of the recently observed positive NAO index trend (Gillett et al., 2003a). Looking for analogues in the past, our record suggests that flood size decreased during warmer climate periods (e.g., Holocene Climatic Optimum, 1.7 ka, 0.9 ka), although flood frequency remained high. In particular, exceptional flood events occurred during past warm/dry conditions, namely at 1.8 ka (11,000 m^3/s) and 8.4 ka (8100 m^3/s), in the context of a highly variable hydroclimate. Therefore, although the frequency of large floods has decreased since mid-20th century in the southwestern Europe, our palaeoflood record indicates that flood outliers are likely to occur in a climate change context.

The Duero palaeoflood record provides direct evidence of extreme weather events and associated paleoclimatic conditions. Other natural archives, such as lacustrine environments and speleothems, can also document discrete flood events either through direct indicators (e.g., flood sands; Wilhelm et al., 2019) or sedimentological and geochemical proxies (e.g., Ben Dor et al., 2021, Corella et al., 2021). Lacustrine environments, in particular, are highly sensitive and can provide continuous records over millennia in stable settings. Reconstructing flood series from lacustrine records is generally straightforward through the identification of detrital layers, but estimating flood magnitudes may necessitate additional proxies, such as bed thickness and grain size, or even calibration with present-day instrumental records (e.g., Kämpf et al., 2015). In contrast, flood sediments deposited on flood benches at different elevations exhibit a natural self-discrimination based on flood palaeostage, offering a direct indication of discharge.

The completeness of the fluvial palaeoflood records is often debated, as many records show bias towards recent times (e.g. Benito et al., 2015c). Our study demonstrates that in fluvial settings with ample storage capacity, such as river confluences, sediment preservation spans millennia with remarkable fidelity. These individual flood extremes in large rivers offer valuable insights into extreme past events, that could be catastrophic if they happen again (Baker et al., 2022). Estimating palaeodischarges under different climate episodes (e.g., Early Holocene, Medieval Climatic Anomaly, and Little Ice Age) is vital for establishing connections between causative synoptic-scale atmospheric patterns and climatic drivers. The distribution of floods in the Duero River and the associated weather extremes exhibit a non-stationary behavior over multi-decadal to centennial time scales, likely attributed to a spatial shift in severe weather conditions towards other Atlantic regions (Fig. 12). In the context of global warming, understanding the spatio-temporal hydroclimatic variability provides robust guidance for assessing flood magnitude possibilities and planning for climate change adaptation.

6. Conclusions

The exceptional physiographic setting of the Duero River gorge (at the Portuguese-Spanish border) makes it an ideal environment for the deposition and preservation of extreme floods over the last 15,000 years, providing a representative record of the long-term atmospheric circulation and climate extremes in the South Atlantic European region. Our key findings are:

- The Duero palaeoflood record consists of 62 floods that exceeded a discharge of ~5000 m^3/s. The palaeoflood record supported by OSL chronologies from multiple sites identified ten flood-rich periods during the last 15 ka. The largest palaeoflood in the study area was dated to 1.8 ± 0.1 ka, provided a minimum discharge of 11,000 m^3/s. For comparison the largest instrumental flood was recorded in 1962 with a discharge of 7300 m^3/s. The discharge error associated with channel bed incision during the Late Pleistocene to Holocene was estimated to range from 115 to 350 m^3/s. This is equivalent to 2–6% of the smallest palaeoflood discharge (5800 m^3/s). Consequently, thisdischarge error has an insignificant impact on the reported palaeodischarges, particularly when considering that flood beds served as minimum palaeostage indicators.
- On a regional scale, flood-rich episodes of the Duero correlate with (1) high stands of nearby lakes (high river discharge inputs) and (2) flood-rich periods of flooding in the Tagus River, the second largest Atlantic river in the Iberian Peninsula. The agreement between flood

periods and wet hydroclimatic indicators suggests an excellent response of flooding to North Atlantic atmospheric circulation variability, mainly driven by negative modes of NAO-like conditions during the Holocene.

- During the Early Holocene, flood-rich periods (ca. 11.5 ka, 10.8–10.3 ka, 9.5 ka) are coherent with spanning frequencies of meltwater pulses (11.4 ka, 10.4 ka and 9.4 ka; Bond et al., 2001). Flood-producing conditions were enhanced by a warmer and saltier North Atlantic Oceanic current that reactivated northward heat transport from tropical and subtropical regions.
- The middle Holocene was characterized by a paucity of large floods, consistent with climate proxies indicating strong westerlies winds and a dominant positive mode of NAO-like circulation
- The Late Holocene flood clusters are associated with centennial periods of weak westerlies and strong Siberian High, leading to atmospheric blocking and persistent negative NAO phases. Some flood episodes correspond to relatively cool temperatures (4.5–4.4 ka, 1.8–1.5 ka, 0.53–0.46 ka and 0.32–0.11 ka), but others overlap with warm conditions (2.4–2.1 ka and 1.1–0.8 ka) in southwestern Europe. This observation suggests that flood-producing processes in south Atlantic Europe have been driven by other atmospheric-ocean coupling conditions rather than by changes in temperature (warm-cold) alone.
- Annual flood peaks have decreased since the mid-20th century coinciding with a shift to a dominant positive winter NAO phase since the 1980s. On a centennial timescale, flood magnitude decreased during past warm climate conditions (Holocene Climatic Optimum, 1.7 ka, 0.9 ka). Nevertheless, the most extreme floods (outliers) occurred during past warm/dry periods, probably reflecting a highly variable hydroclimate.
- The long-term flood distribution shows a non-stationary behavior over multi-decadal to centennial time scales. Despite a decrease in the frequency of large floods in southwestern Europe since mid-20th century, our palaeoflood record indicates that the occurrence of similar flood outliers (>11,000 m^3/s) observed during warm past periods remains a possibility in the context of climate change.

Declaration of competing interest

The authors declare that they have no known competing financial interests or personal relationships that could have appeared to influence the work reported in this paper.

Data availability

Data will be made available on request.

Acknowledgements

We extent our gratitude to Paul Carling and Ian Fuller for their constructive and valuable reviews. We would like to thank to Jose Angel Martinez Pérez, Director of Operations and Management Service at Iberdrola (hydropower company) in Carbajosa de la Sagrada (Salamanca), and by Yolanda Diego Martín, Director of Documentation Management of the Historical Archive of Iberdrola in Ricobayo (Zamora), for their invaluable support in providing hydrological data and documentation. This publication is part of the R + D project PID2020-116537RB-I00 (EPHIDREAMS) funded by MCIN/AEI/10.13039/501100011033, the Spanish General Water Directorate (DGA) of the MITERD (Grant MNCN-CSIC 20223TE002), and the Fundación Biodiversidad (grant PRCV00446). J.P Corella postdoctoral fellowship was funded by the European Union's Horizon 2020 research and innovation programme under the Marie Sklodowska-Curie (MSCA-IF-EF-ST) funding scheme (grant nº 796752).

References

Aires, C., Pereira, D.I., Azevedo, T.M., 2000. Inundações do rio Douro: dados históricos e hidrológicos, I Jornadas do Quarternário da APEQ, Porto.
Alcoforado, M.J., Silva, L.P., Amorim, I., Fragoso, M., Garcia, J.C., 2021. Historical floods of the Douro River in Porto, Portugal (1727–1799). Clim. Change 165, 17.
Alley, R.B., 2000. The Younger Dryas cold interval as viewed from central Greenland. Quat. Sci. Rev. 19, 213–226.
Alonso-Zarza, A.M., Armenteros, I., Braga, J.C., Muñoz, A., Pujalte, V., Ramos, E., Aguirre, J., Alonso-Gavilán, G., Arenas, C., Ignacio Baceta, J., Carballeira, J., Calvo, J.P., Corrochano, A., Fornós, J.J., González, A., Luzón, A., Martín, J.M., pardo, G., payros, A., Pérez, A., Pomar, L., Rodriguez, J.M., Villena, J., Gibbons, W., Moreno, T., 2002. Tertiary, the Geology of Spain. Geological Society of London.
Amorim, I., Garcia, J.C., Silva, L.P., 2017. As cheias do rio Douro no Porto (Portugal) do século XVIII. SÉMATA 29, 185–217.
Antón, L., Rodés, A., de Vicente, G., Pallàs, R., Garcia-Castellanos, D., Stuart, F.M., Braucher, R., Bourlès, D., 2012. Quantification of fluvial incision in the Duero Basin (NW Iberia) from longitudinal profile analysis and terrestrial cosmogenic nuclide concentrations. Geomorphology 165, 50–61. https://doi.org/10.1016/j.geomorph.2011.12.036.
Baker, V.R., 1987. Paleoflood hydrology and extraordinary flood events. J. Hydrol. 96, 79–99.
Baker, V.R., 2008. Paleoflood hydrology: origin, progress, prospects. Geomorphology 101, 1–13.
Baker, V.R., Kochel, R.C., 1988. In: Baker, V.R., Kochel, R.C., Patton, P.C. (Eds.), Flood sedimentation in bedrock fluvial systems, Flood Geomorphology. J. Wiley, New York, pp. 123–137.
Baker, A., Hellstrom, J.C., Kelly, B.F.J., Mariethoz, G., Trouet, V., 2015. A composite annual-resolution stalagmite record of North Atlantic climate over the last three millennia. Sci. Rep. 5 (1), 10307 https://doi.org/10.1038/srep10307.
Baker, V.R., Benito, G., Brown, A.G., Carling, P.A., Enzel, Y., Greenbaum, N., Herget, J., Kale, V.S., Latrubesse, E.M., Macklin, M.G., Nanson, G.C., Oguchi, T., Thorndycraft, V.R., Ben Dor, Y., Zituni, R., 2022. Fluvial palaeohydrology in the 21st century and beyond. Earth Surf. Process. Landforms 47, 58–81.
Bakke, J., Lie, Ø., Heegaard, E., Dokken, T., Haug, G.H., Birks, H.H., Dulski, P., Nilsen, T., 2009. Rapid oceanic and atmospheric changes during the Younger Dryas cold period. Nat. Geosci. 2, 202–205.
Baldini, L.M., Baldini, J.U., McDermott, F., Arias, P., Cueto, M., Fairchild, I.J., Hoffmann, D.L., Mattey, D.P., Müller, W., Nita, D.C., Ontañon, R., García-Moncó, C., Richards, D.A., 2019. North Iberian temperature and rainfall seasonality over the younger Dryas and Holocene. Quat. Sci. Rev. 226, 105998.
Ballesteros-Cánovas, J.A., Stoffel, M., St George, S., Hirschboeck, K., 2015. A review of flood records from tree rings. Prog. Phys. Geogr. 39, 794–816.
Ballesteros-Cánovas, J.A., Stoffel, M., Benito, G., Rohrer, M., Barriopedro, D., García-Herrera, R., Beniston, M., Brönnimann, S., 2019. On the extraordinary winter flood episode over the North Atlantic Basin in 1936. Ann. N. Y. Acad. Sci. 1436, 206–216.
Barriopedro, D., García-Herrera, R., Huth, R., 2008. Solar modulation of Northern Hemisphere winter blocking. J. Geophys. Res. Atmos. 113.
Ben Dor, Y., Armon, M., Ahlborn, M., Morin, E., Erel, Y., Brauer, A., Schwab, M.J., Tjallingii, R., Enzel, Y., 2018. Changing flood frequencies under opposing Late Pleistocene eastern Mediterranean climates. Sci. Rep. 8.
Ben Dor, Y., Flax, T., Levitan, I., Enzel, Y., Brauer, A., Erel, Y., 2021. The paleohydrological implications of aragonite precipitation under contrasting climates in the endorheic Dead Sea and its precursors revealed by experimental investigations. Chem. Geol. 576, 120261.
Benito, G., Díez-Herrero, A., Fernández De Villalta, M., 2003a. Magnitude and frequency of flooding in the Tagus basin (Central Spain) over the last millennium. Clim. Change 58, 171–192.
Benito, G., Sopena, A., Sanchez-Moya, Y., Machado, M.J., Perez-Gonzalez, A., 2003b. Palaeoflood record of the Tagus River (Central Spain) during the late Pleistocene and Holocene. Quat. Sci. Rev. 22, 1737–1756.
Benito, G., Brazdil, R., Herget, J., Machado, M.J., 2015a. Quantitative historical hydrology in Europe. Hydrol. Earth Syst. Sci. 19, 3517–3539.
Benito, G., Macklin, M.G., Panin, A., Rossato, S., Fontana, A., Jones, A.F., Machado, M.J., Matlakhova, E., Mozzi, P., Zielhofer, C., 2015b. Recurring flood distribution patterns related to short-term Holocene climatic variability. Sci. Rep. 5, 16398.
Benito, G., Macklin, M.G., Zielhofer, C., Jones, A.F., Machado, M.J., 2015c. Holocene flooding and climate change in the Mediterranean. Catena 130, 13–33.
Benito, G., Harden, T.M., O'Connor, J.E., 2020. In: Wohl, E. (Ed.), Quantitative paleoflood hydrology, second ed. ed., ☆, Reference Module in Earth Systems and Environmental Sciences. Elsevier, p. 22pp.
Benito, G., Castillo, O., Ballesteros-Cánovas, J.A., Machado, M., Barriendos, M., 2021. Enhanced flood hazard assessment beyond decadal climate cycles based on centennial historical data (Duero basin, Spain). Hydrol. Earth Syst. Sci. 25, 6107–6132.
Berger, A.L., 1978. Long-term variations of daily insolation and Quaternary climatic changes. J. Atmos. Sci. 35, 2362–2367.
Berger, A., Loutre, M.F., 1991. Insolation values for the climate of the last 10 million years. Quat. Sci. Rev. 10, 297–317.
Bond, G., Kromer, B., Beer, J., Muscheler, R., Evans, M.N., Showers, W., Hoffmann, S., Lotti-Bond, R., Hajdas, I., Bonani, G., 2001. Persistent solar influence on North Atlantic climate during the Holocene. Science 294, 2130–2136.
Came, R.E., Oppo, D.W., McManus, J.F., 2007. Amplitude and timing of temperature and salinity variability in the subpolar North Atlantic over the past 10 k.y. Geology 35, 315–318.

Carrión, J.S., 2002. Patterns and processes of Late Quaternary environmental change in a montane region of southwestern Europe. Quat. Sci. Rev. 21, 2047–2066.
Corella, J.P., Stefanova, V., El Anjoumi, A., Rico, E., Giralt, S., Moreno, A., Plata-Montero, A., Valero-Garcés, B.L., 2013. A 2500-year multi-proxy reconstruction of climate change and human activities in northern Spain: the Lake Arreo record. Palaeogeogr. Palaeoclimatol. Palaeoecol. 386, 555–568.
Corella, J.P., Valero-Garcés, B.L., Vicente-Serrano, S.M., Brauer, A., Benito, G., 2016. Three millennia of heavy rainfalls in Western Mediterranean: frequency, seasonality and atmospheric drivers. Sci. Rep. 6, 38206.
Corella, J.P., Benito, G., Monteoliva, A.P., Sigro, J., Calle, M., Valero-Garcés, B.L., Stefanova, V., Rico, E., Favre, A.C., Wilhelm, B., 2021. A 1400-years flood frequency reconstruction for the Basque country (N Spain): Integrating geological, historical and instrumental datasets. Quat. Sci. Rev. 262, 106963.
Cortesi, N., Trigo, R.M., Gonzalez-Hidalgo, J.C., Ramos, A.M., 2013. Modelling monthly precipitation with circulation weather types for a dense network of stations over Iberia. Hydrol. Earth Syst. Sci. 17, 665–678.
Cunha, P.P., Martins, A.A., Gomes, A., Stokes, M., Cabrale, J., Lopes, F.C., Pereira, D., de Vicente, Gerardo, Buylaert, J.P., Murray, A.S., Ant'on, L., 2019. Mechanisms and age estimates of continental-scale endorheic to exorheic drainage transition: Douro RiverWestern Iberia. Global Planet. Change 181, 102985. https://doi.org/10.1016/j.gloplacha.2019.102985.
Daveau, S., 1978. Os temporais de Fevereiro/Março de 1978. Finisterra 13.
Daveau, S., 1988. In: João Sá da Costa, Lisboa (Ed.), Geografia de Portugal. II. O ritmo climático e a paisagem, Colaboration with H. Lautensach and O. Ribeiro), pp. 335–623.
Davis, B.A.S., Brewer, S., Stevenson, A.C., Guiot, J., 2003. The temperature of Europe during the Holocene reconstructed from pollen data. Quat. Sci. Rev. 22, 1701–1716.
de Abreu, L., Shackleton, N.J., Schönfeld, J., Hall, M., Chapman, M., 2003. Millennial-scale oceanic climate variability off the Western Iberian margin during the last two glacial periods. Mar. Geol. 196, 1–20.
Denniston, R.F., Luetscher, M., 2017. Speleothems as high-resolution paleoflood archives. Quat. Sci. Rev. 170, 1–13.
Drago, T., Freitas, C., Rocha, F., Moreno, J., Cachão, M., Naughton, F., Fradique, C., Araújo, F., Silveira, T., Oliveira, A., Cascalho, J., Fatela, F., 2006. Paleoenvironmental evolution of estuarine systems during the last 14000 Years - the case of Douro estuary (NW Portugal). J. Coast Res. 186–192.
Durcan, J., King, G., Duller, G.A.T., 2015. DRAC: dose rate and age calculator for trapped charge dating. Quat. Geochronol. 28, 54–61.
Ely, L.L., Enzel, Y., Baker, V.R., Kale, V.S., Mishra, S., 1996. Changes in the magnitude and frequency of late Holocene monsoon floods on the Narmada River, central India. Geol. Soc. Am. Bull. 108, 1134–1148.
Hydrologic Engineering Center, 2010. HEC-RAS, River Analysis System, Hydraulics Version 4.1. US. Army Corps of Engineers, Davis, CA, p. 411.
Enzel, Y., 1992. Flood frequency of the Mojave River and the formation of late Holocene Playa lakes, southern California, USA. Holocene 2, 11–18.
Feinberg, J.M., Lascu, I., Lima, E.A., Weiss, B.P., Dorale, J.A., Alexander, E.C., Edwards, R.L., 2019. Magnetic detection of paleoflood layers in stalagmites and implications for historical land use changes. Earth Planet Sci. Lett., 115946
Galbraith, R.F., Roberts, R.G., Laslett, G.M., Yoshida, H., Olley, J.M., 1999. Optical dating of single and multiple grains of quartz from Jinmium rock shelter, Northern Australia: Part I, experimental design and statistical models. Archaeometry 41, 339–364.
Gillett, N.P., Graf, H.F., Osborn, T.J., 2003a. Climate Change and the North Atlantic Oscillation, the North Atlantic Oscillation. Climatic Significance and Environmental Impact, pp. 193–209.
Gillett, N.P., Zwiers, F.W., Weaver, A.J., Stott, P.A., 2003b. Detection of human influence on sea-level pressure. Nature 422, 292–294.
Gimeno, L., de la Torre, L., Nieto, R., García, R., Hernández, E., Ribera, P., 2003. Changes in the relationship NAO-Northern hemisphere temperature due to solar activity. Earth Planet Sci. Lett. 206, 15–20.
Gonzalez-Lemos, S., Müller, W., Pisonero, J., Cheng, H., Edwards, R., Heather, S., 2015. Holocene flood frequency reconstruction from speleothems in northern Spain. Quat. Sci. Rev. 127, 129–140.
González-Sampériz, P., Valero-Garcés, B.L., Moreno, A., Jalut, G., García-Ruiz, J.M., Martí-Bono, C., Delgado-Huertas, A., Navas, A., Otto, T., Dedoubat, J.J., 2006. Climate variability in the Spanish Pyrenees during the last 30,000 yr revealed by the El Portalet sequence. Quat. Res. 66, 38–52.
Goy, J.L., Rodríguez López, G., Martínez-Graña, A.M., Cruz, R., Valdés, V., 2019. Geomorphological analysis applied to the evolution of the quaternary landscape of the Tormes River (Salamanca, Spain). Sustainability 11, 7255. https://doi.org/10.3390/su11247255.
Greenbaum, N., Harden, T.M., Baker, V.R., Weisheit, J., Cline, M.L., Porat, N., Halevi, R., Dohrenwend, J., 2014. A 2000 year natural record of magnitudes and frequencies for the largest Upper Colorado River floods near Moab, Utah. Water Resour. Res. 50, 5249–5269.
Häkkinen, S., Rhines, P.B., Worthen, D.L., 2011. Atmospheric blocking and Atlantic multidecadal ocean variability. Science 80 (334), 655–659.
Hátún, H., Sandø, A.B., Drange, H., Hansen, B., Valdimarsson, H., 2005. Influence of the Atlantic subpolar Gyre on the thermohaline circulation. Science 309, 1841–1844.
Helama, S., Jones, P.D., Briffa, K.R., 2017. Dark Ages Cold Period: a literature review and directions for future research. Holocene 27, 1600–1606.
Hurrell, J.W., 1995. Decadal trends in the North Atlantic oscillation: regional temperatures and precipitation. Science 269, 676–679.
Hurrell, J.W., Kushnir, Y., Ottersen, G., Visbeck, M., 2003. In: Hurrell, J.W., Kushnir, Y., Ottersen, G., Visbeck, M. (Eds.), An overview of the North Atlantic oscillation, The North Atlantic Oscillation: Climatic Significance and Environmental Impact. Geophysical Monograph Series. AGU, pp. 1–35. https://doi.org/10.1029/134GM01.
Iberduero, S.A., 1953. Proyecto de construcción del Salto de Saucelle en el tramo internacional del Río Duero, p. 235. Bilbao.
Iberduero, S.A., 1956. Proyecto de Construcción del Salto de Adeadávila en el tramo internacional del Río Duero, p. 115. Bilbao.
Jalut, G., Esteban Amat, A., Bonnet, L., Gauquelin, T., Fontugne, M., 2000. Holocene climatic changes in the Western Mediterranean, from south-east France to south-east Spain. Palaeogeogr. Palaeoclimatol. Palaeoecol. 160, 255–290.
Jambrina-Enríquez, M., Rico, M., Moreno, A., Leira, M., Bernárdez, P., Prego, R., Recio, C., Valero-Garcés, B., 2014. Timing of deglaciation and postglacial environmental dynamics in NW Iberia: the Sanabria Lake record. Quat. Sci. Rev. 94, 136–158.
Jambrina-Enríquez, M., Sachse, D., Valero-Garcés, B.L., 2016. A deglaciation and Holocene biomarker-based reconstruction of climate and environmental variability in NW Iberian Peninsula: the Sanabria Lake sequence. J. Paleolimnol. 56, 49–66.
Jiménez Cisneros, B.E., Oki, T., Arnell, N.W., Benito, G., Cogley, J.G., Döll, P., Jiang, T., Mwakalila, S.S., 2014. In: Field, C.B., Barros, V.R., Dokken, D.J., Mach, K.J., Mastrandrea, M.D., Bilir, T.E., Chatterjee, M., Ebi, K.L., Estrada, Y.O., Genova, R.C., Girma, B., Kissel, E.S., Levy, A.N., MacCracken, S., Mastrandrea, P.R., White, L.L. (Eds.), Freshwater resources, Climate Change 2014: Impacts, Adaptation, and Vulnerability. Part A: Global and Sectoral Aspects. Contribution of Working Group II to the Fifth Assessment Report of the Intergovernmental Panel of Climate Change. Cambridge University Press, Cambridge, United Kingdom and New York, NY, USA, pp. 229–269.
Jones, A.F., Macklin, M.G., Benito, G., 2015. Meta-analysis of Holocene fluvial sedimentary archives: a methodological primer. Catena 130, 3–12.
Kämpf, L., Mueller, P., Höllerer, H., Plessen, B., Naumann, R., Thoss, H., Güntner, A., Merz, B., Brauer, A., 2015. Hydrological and sedimentological processes of flood layer formation in Lake Mondsee. Depos. Rec. 1, 18–37.
Kochel, R.C., Baker, V.R., 1982. Paleoflood hydrology. Science 215, 353–361.
Kundzewicz, Z.W., Kanae, S., Seneviratne, S.I., Handmer, J., Nicholls, N., Peduzzi, P., Mechler, R., Bouwer, L.M., Arnell, N., Mach, K., Muir-Wood, R., Brakenridge, G.R., Kron, W., Benito, G., Honda, Y., Takahashi, K., Sherstyukov, B., 2014. Flood risk and climate change: global and regional perspectives. Hydrol. Sci. J. 59, 1–28.
Larsen, I.J., Lamb, M.P., 2016. Progressive incision of the Channeled Scablands by outburst floods. Nature 538, 229.
Lewin, J., Macklin, M.G., 2003. Preservation potential for Late Quaternary river alluvium. J. Quat. Sci. 18, 107–120.
Li, X., Huang, C.C., 2017. Holocene palaeoflood events recorded by slackwater deposits along the Jin-Shan Gorges of the middle Yellow River, China. Quat. Int. 453, 85–95.
Liberato, M.L.R., Pinto, J.G., Trigo, R.M., Ludwig, P., Ordóñez, P., Yuen, D., Trigo, I.F., 2013. Explosive development of winter storm Xynthia over the subtropical North Atlantic ocean. Nat. Hazards Earth Syst. Sci. 13, 2239–2251.
Liu, T., Huang, C.C., Pang, J., Zha, X., Zhou, Y., Zhang, Y., Ji, L., 2015. Late Pleistocene and Holocene palaeoflood events recorded by slackwater deposits in the upper Hanjiang River valley, China. J. Hydrol. 529, 499–510.
Lohmann, G., Lorenz, S., 2000. On the hydrological cycle under paleoclimatic conditions as derived from AGCM simulations. J. Geophys. Res. Atmos. 105, 17417–17436.
Lorenzo-Lacruz, J., Vicente-Serrano, S.M., López-Moreno, J.I., González-Hidalgo, J.C., Morán-Tejeda, E., 2011. The response of Iberian rivers to the North Atlantic oscillation. Hydrol. Earth Syst. Sci. 15, 2581–2597.
Loureiro, A., 1904. Portos marítimos de Portugal e Ilhas Adjacentes. Imprensa Nacional, Lisboa, Portugal.
Macklin, M.G., Benito, G., Gregory, K.J., Johnstone, E., Lewin, J., Michczyńska, D.J., Soja, R., Starkel, L., Thorndycraft, V.R., 2006. Past hydrological events reflected in the Holocene fluvial record of Europe. Catena 66, 145–154.
Magny, M., Combourieu-Nebout, N., de Beaulieu, J.L., Bout-Roumazeilles, V., Colombaroli, D., Desprat, S., Francke, A., Joannin, S., Ortu, E., Peyron, O., Revel, M., Sadori, L., Siani, G., Sicre, M.A., Samartin, S., Simonneau, A., Tinner, W., Vannière, B., Wagner, B., Zanchetta, G., Anselmetti, F., Brugiapaglia, E., Chapron, E., Debret, M., Desmet, M., Didier, J., Essallami, L., Galop, D., Gilli, A., Haas, J.N., Kallel, N., Millet, L., Stock, A., Turon, J.L., Wirth, S., 2013. North–south palaeohydrological contrasts in the central Mediterranean during the Holocene: tentative synthesis and working hypotheses. Clim. Past 9, 2043–2071.
Marino Alfonso, J.L., Poblete Piedrabuena, M.A., Beato Bergua, S., 2018. Geomorfología de los Arribes del Duero zamoranos. Estud. Geográficos 79, 419–444.
Martin Serrano, A., 1991. La definicion y el encajamiento de la red fluvial actual sobre el macizo Hesperico en el marco de su geodinamica alpina. Rev. Soc. Geol. Espana 4, 337–351.
Martin-Puertas, C., Matthes, K., Brauer, A., Muscheler, R., Hansen, F., Petrick, C., Aldahan, A., Possnert, G., van Geel, B., 2012. Regional atmospheric circulation shifts induced by a grand solar minimum. Nat. Geosci. 5, 397–401.
Mayewski, P.A., Meeker, L.D., Twickler, M.S., Whitlow, S., Yang, Q., Lyons, W.B., Prentice, M., 1997. Major features and forcing of high-latitude northern hemisphere atmospheric circulation using a 110,000-year-long glaciochemical series. J. Geophys. Res.: Oceans 102, 26345–26366.
Mayewski, P.A., Rohling, E.E., Curt Stager, J., Karlén, W., Maasch, K.A., David Meeker, L., Meyerson, E.A., Gasse, F., van Kreveld, S., Holmgren, K., Lee-Thorp, J., Rosqvist, G., Rack, F., Staubwasser, M., Schneider, R.R., Steig, E.J., 2004. Holocene climate variability. Quat. Res. 62, 243–255.
McManus, J.F., Francois, R., Gherardi, J.M., Keigwin, L.D., Brown-Leger, S., 2004. Collapse and rapid resumption of Atlantic meridional circulation linked to deglacial climate changes. Nature 428, 834–837.

Medialdea, A., Thomsen, K.J., Murray, A.S., Benito, G., 2014. Reliability of equivalent-dose determination and age-models in the OSL dating of historical and modern palaeoflood sediments. Quat. Geochronol. 22, 11–24.
MMA, M.d.M.A., 2011. Guía Metodológica para el desarrollo del Sistema Nacional de Cartografía de Zonas Inundables. Ministerio de Medio Ambiente y Medio Rural y Marino, Madrid, Spain.
Mohr, S., Ehret, U., Kunz, M., Ludwig, P., Caldas-Alvarez, A., Daniell, J.E., Ehmele, F., Feldmann, H., Franca, M.J., Gattke, C., Hundhausen, M., Knippertz, P., Küpfer, K., Mühr, B., Pinto, J.G., Quinting, J., Schäfer, A.M., Scheibel, M., Seidel, F., Wisotzky, C., 2022. A multi-disciplinary analysis of the exceptional flood event of July 2021 in central Europe. Part 1: event description and analysis. Nat. Hazards Earth Syst. Sci. Discuss. 2022, 1–44.
Morán-Tejeda, E., Ceballos-Barbancho, A., Llorente-Pinto, J.M., López-Moreno, J.I., 2012. Land-cover changes and recent hydrological evolution in the Duero Basin (Spain). Reg. Environ. Change 12, 17–33.
Morellón, M., Valero-Garcés, B.L., Caballud, A.M., González-Sampériz, P., Mata, M.P., Romero, Ó.E., Martínez, M.M., Izquierdo, A.N., Izquierdo, A.N., 2008. Holocene Palaeohydrology and Climate Variability in Northeastern Spain: the Sedimentary Record of Lake Estanya (Pre-pyrenean Range). Elsevier.
Morellón, M., Valero-Garcés, B., Vegas-Vilarrúbia, T., González-Sampériz, P., Romero, Ó., Delgado-Huertas, A., Mata, P., Moreno, A., Rico, M., Corella, J.P., 2009. Lateglacial and Holocene palaeohydrology in the western Mediterranean region: the Lake Estanya record (NE Spain). Quat. Sci. Rev. 28, 2582–2599.
Morellón, M., Aranbarri, J., Moreno, A., González-Sampériz, P., Valero-Garcés, B.L., 2018. Early Holocene humidity patterns in the Iberian Peninsula reconstructed from lake, pollen and speleothem records. Quat. Sci. Rev. 181, 1–18.
Moreno, A., López-Merino, L., Leira, M., Marco-Barba, J., González-Sampériz, P., Valero-Garcés, B.L., López-Sáez, J.A., Santos, L., Mata, P., Ito, E., 2011. Revealing the last 13,500 years of environmental history from the multiproxy record of a mountain lake (Lago Enol, northern Iberian Peninsula). J. Paleolimnol. 46, 327–349.
Moreno, A., Pérez-Mejías, C., Bartolomé, M., Sancho, C., Cacho, I., Stoll, H., Delgado-Huertas, A., Hellstrom, J., Edwards, R.L., Cheng, H., 2017. New speleothem data from Molinos and Ejulve caves reveal Holocene hydrological variability in northeast Iberia. Quat. Res. 88, 223–233.
Muñoz Sobrino, C., Ramil-Rego, P., Rodríguez Guitián, M.A., 2001. Vegetation in the mountains of northwest Iberia during the last glacial-interglacial transition. Veg. Hist. Archaeobotany 10, 7–21.
Muñoz Sobrino, C., Ramil-Rego, P., Gómez-Orellana, L., 2007. Late Würm and early Holocene in the mountains of northwest Iberia: biostratigraphy, chronology and tree colonization. Veg. Hist. Archaeobotany 16, 223–240.
Muñoz Sobrino, C., Heiri, O., Hazekamp, M., van der Velden, D., Kirilova, E.P., García-Moreiras, I., Lotter, A.F., 2013. New data on the Lateglacial period of SW Europe: a high resolution multiproxy record from Laguna de la Roya (NW Iberia). Quat. Sci. Rev. 80, 58–77.
Naughton, F., Silveira, T., Rocha, F., Drago, T., 2005. Palaeoenviromental analysis of Douro estuary based on mineralogical parameters. Thalassas 21, 53–58.
Naughton, F., Sánchez Goñi, M.F., Drago, T., Freitas, M.C., Oliveira, A., 2007. Holocene changes in the Douro estuary (northwestern Iberia). J. Coast Res. 23, 711–720.
Naughton, F., Sanchez Goñi, M.F., Rodrigues, T., Salgueiro, E., Costas, S., Desprat, S., Duprat, J., Michel, E., Rossignol, L., Zaragosi, S., Voelker, A.H.L., Abrantes, F., 2016. Climate variability across the last deglaciation in NW Iberia and its margin. Quat. Int. 414, 9–22.
Noren, A.J., Bierman, P.R., Steig, E.J., Lini, A., Southon, J., 2002. Millennial-scale storminess variability in the northeastern United States during the Holocene epoch. Nature 419, 821–824.
Olsen, J., Anderson, N.J., Knudsen, M.F., 2012. Variability of the North Atlantic oscillation over the past 5,200 years. Nat. Geosci. 5, 808–812.
Ortega, J.A., Garzon, G., 2002. Palaeohydrology of the Lower Guadiana River Basin.
Ortega-Becerril, J.A., Garrote, J., 2023. Magnitude of formative flows in stream potholes. Geomorphology 434, 108738.
O'Connor, J.E., Grant, G.E., Costa, J.E., 2002. In: House, P.K., Webb, R.H., Baker, V.R., Levish, D.R. (Eds.), The geology and geography of floods, Ancient Floods, Modern Hazards. Principles and Applications of Paleoflood Hydrology, vol. 5. American Geophysical Union Water Science and Application Series, pp. 359–385.
Pardé, M., 1967. Les crues remarquables du Douro inférieur. Rev. Geogr. Pyrenees Sud-Ouest 38, 231–242.
Pereira, S., Ramos, A.M., Zêzere, J.L., Trigo, R.M., Vaquero, J.M., 2016. Spatial impact and triggering conditions of the exceptional hydro-geomorphological event of December 1909 in Iberia. Nat. Hazards Earth Syst. Sci. 16, 371–390.
Perşoiu, A., Ionita, M., Weiss, H., 2019. Atmospheric blocking induced by the strengthened Siberian High led to drying in west Asia during the 4.2 ka BP event – a hypothesis. Clim. Past 15, 781–793.
Prescott, J.R., Hutton, J.T., 1994. Cosmic ray contributions to dose rates for luminescence and ESR dating: large depths and long-term time variations. Radiat. Meas. 23, 497–500.
Ramos, A.M., Trigo, R.M., Liberato, M.L.R., Tomé, R., 2015. Daily precipitation extreme events in the Iberian Peninsula and its association with atmospheric rivers. J. Hydrometeorol. 16, 579–597.
Ramsey, C.B., 2001. Development of the radiocarbon Program OxCal. Radiocarbon 43, 355–363.
Reimer, P.J., Austin, W.E.N., Bard, E., Bayliss, A., Blackwell, P.G., Bronk Ramsey, C., Butzin, M., Cheng, H., Edwards, R.L., Friedrich, M., Grootes, P.M., Guilderson, T.P., Hajdas, I., Heaton, T.J., Hogg, A.G., Hughen, K.A., Kromer, B., Manning, S.W., Muscheler, R., Palmer, J.G., Pearson, C., van der Plicht, J., Reimer, R.W., Richards, D.A., Scott, E.M., Southon, J.R., Turney, C.S.M., Wacker, L., Adolphi, F., Büntgen, U., Capano, M., Fahrni, S.M., Fogtmann-Schulz, A., Friedrich, R., Köhler, P., Kudsk, S., Miyake, F., Olsen, J., Reinig, F., Sakamoto, M., Sookdeo, A., Talamo, S., 2020. The IntCal20 northern hemisphere radiocarbon age calibration curve (0–55 cal kBP). Radiocarbon 62, 725–757.
Repschläger, J., Garbe-Schönberg, D., Weinelt, M., Schneider, R., 2017. Holocene evolution of the North Atlantic subsurface transport. Clim. Past 13, 333–344.
Rimbu, N., Boroneanţ, C., Buţă, C., Dima, M., 2002. Decadal variability of the Danube river flow in the lower basin and its relation with the North Atlantic Oscillation. Int. J. Climatol. 22, 1169–1179. https://doi.org/10.1002/joc.788.
Rimbu, N., Lohmann, G., Kim, J.-H., Arz, H.W., Schneider, R., 2003. Arctic/North Atlantic Oscillation signature in Holocene sea surface temperature trends as obtained from alkenone data. Geophys. Res. Lett. 30, 1280. https://doi.org/10.1029/2002GL016570.
Roca, J.R., Juliá, R., 1997. Late-glacial and Holocene lacustrine evolution based on ostracode assemblages in Southeastern Spain. Geobios 30, 823–830.
Rocha, F., Drago, T., Naughton, F., Silveira, T., 2002. Palaeoenvironmental analysis of Douro Estuary based on mineralogical parameters. Thalassas 21, 53–58.
Rocha, F., Drago, T., Naughton, F., Silveira, T., 2005. Palaeoenvironmental analysis of Douro Estuary based on mineralogical parameters. Thalassas 21, 53–58.
Rodrigo, F.S., 2021. Exploring combined influences of seasonal east Atlantic (EA) and North Atlantic oscillation (NAO) on the temperature-precipitation relationship in the Iberian Peninsula. Geosciences 11, 211.
Rodríguez-Rodríguez, L., Antón, L., Rodés, Á., Pallàs, R., García-Castellanos, D., Jiménez-Munt, I., Struth, L., Leanni, L., Aumaître, G., Bourlès, D., Keddadouche, K., 2020. Dates and rates of endo-exorheic drainage development: insights from fluvial terraces (Duero River, Iberian Peninsula). Global Planet. Change 193, 103271.
Roggenkamp, T., Herget, J., 2014. Reconstructing peak discharges of historic floods of the river Ahr, Germany. Erdkunde 68, 49–59.
Roggenkamp, T., Herget, J., 2022. Hochwasser der Ahr im Juli 2021 –Abflusseinschätzung und Einordnung. Hydrol. Wasserbewirtsch. (HyWa) 66, 40–49.
Salgueiro, A.R., Machado, M.J., Barriendos, M., Pereira, H.G., Benito, G., 2013. Flood magnitudes in the Tagus River (Iberian Peninsula) and its stochastic relationship with daily North Atlantic oscillation since mid-19th century. J. Hydrol. 502, 191–201.
Santisteban, J.I., Alcala, L., Mediavilla, R.M., Alberdi, M.T., Luque, L., Mazo, A., Miguel, I., Morales, J., Perez, B., 1996. El yacimiento de Tariego de Cerrato; el inicio de la red fluvial actual en el sector de la cuenca del Duero. Cuad. Geol. Iber. 22, 431–446.
Santos, L., Romani, J.R.V., Jalut, G., 2000. History of vegetation during the Holocene in the Courel and queixa Sierras, Galicia, northwest Iberian Peninsula. J. Quat. Sci. 15, 621–632.
Schaller, M., Ehlers, T.A., Stor, T., Torrent, J., Lobato, L., Christl, M., Vockenhuber, C., 2016. Timing of European fluvial terrace formation and incision rates constrained by cosmogenic nuclide dating. Earth Planet Sci. Lett. 451, 221–231. https://doi.org/10.1016/j.epsl.2016.0.022.
Schillereff, D.N., Chiverrell, R.C., Macdonald, N., Hooke, J.M., 2016. Hydrological thresholds and basin control over paleoflood records in lakes. Geology 44, 43–46.
Schott, F.A., Zantopp, R., Stramma, L., Dengler, M., Fischer, J.R., Wibaux, M., 2004. Circulation and deep-water Export at the western Exit of the subpolar North Atlantic. J. Phys. Oceanogr. 34 (2004), 817–843.
Shabbar, A., Huang, J., Higuchi, K., 2001. The relationship between the wintertime north Atlantic oscillation and blocking episodes in the north Atlantic. Int. J. Climatol. 21, 355–369. https://doi.org/10.1002/joc.612.
Silva, J., Oliveira, M., 2002. In: Seville, U.o. (Ed.), As cheias na parte portuguesa da bacia hidrográfica do rio Douro, III Congreso Ibérico sobre gestión y planificación del agua: "La Directiva Marco del Agua: realidades y futuros". Fundación Nueva Cultura del Agua, Sevilla, Spain, p. 16.
Sridhar, A., 2007. A mid–late Holocene flood record from the alluvial reach of the Mahi River, Western India. Catena 70, 330–339.
Stanev, E.V., Peneva, E.L., 2001. Regional sea level response to global climatic change: black Sea examples. Global Planet. Changes 32, 33–47. https://doi.org/10.1016/S0921-8181(01)00148-5.
Struth, L., Garcia-Castellanos, D., Viaplana-Muzas, M., Vergés, J., 2019. Drainage network dynamics and knickpoint evolution in the Ebro and Duero basins: from endorheism to exorheism. Geomorphology 327, 554–571. https://doi.org/10.1016/j.geomorph.2018.11.033.
Thatcher, D.L., Wanamaker, A.D., Denniston, R.F., Asmerom, Y., Polyak, V.J., Fullick, D., Ummenhofer, C.C., Gillikin, D.P., Haws, J.A., 2020. Hydroclimate variability from western Iberia (Portugal) during the Holocene: insights from a composite stalagmite isotope record. Holocene 30, 966–981.
Thomsen, K.J., Murray, A.S., Bøtter-Jensen, L., Kinahan, J., 2007. Determination of burial dose in incompletely bleached fluvial samples using single grains of quartz. Radiat. Meas. 42, 370–379.
Thornalley, D.J.R., Elderfield, H., McCave, I.N., 2009. Holocene oscillations in temperature and salinity of the surface subpolar North Atlantic. Nature 457, 711–714.
Trenberth, K.E., Jones, P.D., Ambenje, P., Bojariu, R., Easterling, D., Klein Tank, A., Parker, D., Rahimzadeh, F., Renwick, J.A., Rusticucci, M., Soden, B., Zhai, P., 2007. In: Solomon, S., D, Q., Manning, M., Chen, Z., Marquis, M., Averyt, K.B., Tignor, M., Miller, H.L. (Eds.), Observations: surface and atmospheric climate change, Climate Change 2007: the Physical Science Basis. Contribution of Working Group I to the Fourth Assessment Report of the Intergovernmental Panel on Climate Change. Cambridge University Press, Cambridge, United Kingdom and New York, NY, USA, p. 235 336.

Trigo, I.F., 2006. Climatology and interannual variability of storm-tracks in the Euro-Atlantic sector: a comparison between ERA-40 and NCEP/NCAR reanalyses. Clim. Dynam. 26, 127–143.
Trigo, R.M., Gimeno, L., 2009. In: Letcher, T.M. (Ed.), Chapter 8 - weather pattern changes in the tropics and mid-latitudes as an indicator of global changes, Climate Change. Elsevier, Amsterdam, pp. 165–180.
Trigo, R.M., Pozo-Vázquez, D., Osborn, T.J., Castro-Díez, Y., Gámiz-Fortis, S., Esteban-Parra, M.J., 2004a. North Atlantic oscillation influence on precipitation, river flow and water resources in the Iberian Peninsula. Int. J. Climatol. 24, 925–944.
Trigo, R.M., Trigo, I.F., DaCamara, C.C., Osborn, T.J., 2004b. Climate impact of the European winter blocking episodes from the NCEP/NCAR Reanalyses. Clim. Dynam. 23, 17–28.
Trigo, R., Varino, F., Ramos, A., Valente, M., Zêzere, J., Vaquero, J., Gouveia, C., Russo, A., 2014. The record precipitation and flood event in Iberia in December 1876: description and synoptic analysis. Front. Earth Sci. 2.
Trouet, V., Esper, J., Graham, N.E., Baker, A., Scourse, J.D., Frank, D.C., 2009. Persistent positive North Atlantic Oscillation mode dominated the medieval climate anomaly. Science 324 (5923), 78–80. https://doi.org/10.1126/science.1166349.
Tukey, J.W., 1977. Exploratory Data Analysis. Addison Wesley, Reading, Mass.
Van Geel, B., Van Der Plicht, J., Kilian, M.R., Klaver, E.R., Kouwenberg, J.H.M., Renssen, H., Reynaud-Farrera, I., Waterbolk, H.T., 1998. The sharp rise of Δ14C ca. 800 cal BC: Possible Causes, related climatic teleconnections and the impact on human environments. Radiocarbon 40, 535–550.
Vannière, B., Magny, M., Joannin, S., Simonneau, A., Wirth, S.B., Hamann, Y., Chapron, E., Gilli, A., Desmet, M., Anselmetti, F.S., 2013. Orbital changes, variation in solar activity and increased anthropogenic activities: controls on the Holocene flood frequency in the Lake Ledro area, Northern Italy. Clim. Past 9, 1193–1209.
Vaquero, J.M., 2004. Solar signal in the number of floods recorded for the Tagus River basin over the last millennium. Climatic Change 66, 23–26.
Vis, G.-J., Bohncke, S.J.P., Schneider, H., Kasse, C., Coenraads-Nederveen, S., Zuurbier, K., Rozema, J., 2010. Holocene flooding history of the lower Tagus valley (Portugal). J. Quat. Sci. 25, 1222–1238.
Visbeck, M.H., Hurrell, J.W., Polvani, L., Cullen, H.M., 2001. The North Atlantic oscillation: past, present, and future. Proc. Natl. Acad. Sci. USA 98 (12), 876–877. https://doi.org/10.1073/pnas.231391598.
Whipple, K.X., Hancock, G.S., Anderson, R.S., 2000. River incision into bedrock: Mechanics and relative efficacy of plucking, abrasion, and cavitation. GSA Bull. 112 (3), 490–503.
Wilhelm, B., Ballesteros Canovas, J.A., Corella Aznar, J.P., Kämpf, L., Swierczynski, T., Stoffel, M., Støren, E., Toonen, W., 2018. Recent advances in paleoflood hydrology: from new archives to data compilation and analysis. Water Secur. 3, 1–8.
Wilhelm, B., Ballesteros Cánovas, J.A., Macdonald, N., Toonen, W.H.J., Baker, V., Barriendos, M., Benito, G., Brauer, A., Corella, J.P., Denniston, R., Glaser, R., Ionita, M., Kahle, M., Liu, T., Luetscher, M., Macklin, M., Mudelsee, M., Munoz, S., Schulte, L., St George, S., Stoffel, M., Wetter, O., 2019. Interpreting historical, botanical, and geological evidence to aid preparations for future floods. Wiley Interdiscipl. Rev.: Water 6, e1318.
Wolf, D., Faust, D., 2015. Western Mediterranean environmental changes: Evidences from fluvial archives. Quat. Sci. Rev. 122.
Wolf, D., Seim, A., Olmo, F., Faust, D., 2013. Late quaternary fluvial dynamics of the Jarama River in central Spain. Quat. Int. 302.
Wolf, D., Seim, A., Faust, D., 2014. Fluvial system response to external forcing and human impact - late Pleistocene and Holocene fluvial dynamics of the lower Guadalete River in western Andalucía (Spain). Boreas 43.
Yang, D.Y., Yu, G., Xie, Y.B., Zhan, D.J., Li, Z.J., 2000. Sedimentary records of large Holocene floods from the middle reaches of the Yellow River, China. Geomorphology 33, 73–88.
Yanosky, T.M., Jarrett, R.D., 2002. In: House, P.K., Webb, R.H., Baker, V.R., Levish, D.R. (Eds.), Dendrochronologic evidence for the frequency and magnitud of paleofloods, Ancient Floods, Modern Hazards: Principles and Applications of Paleoflood Hydrology. Water Science and Application Series, vol. 5. American Geophysical Union, Washington, DC, pp. 77–89.
Zhou, L., Huang, C.C., Zhou, Y., Pang, J., Zha, X., Xu, J., Zhang, Y., Guo, Y., 2016. Late Pleistocene and Holocene extreme hydrological event records from slackwater flood deposits of the Ankang east reach in the upper Hanjiang River valley, China. Boreas 45, 673–687.
Zveryaev, I.I., 2006. Seasonally varying modes in long-term variability of European precipitation during the 20th century. J. Geophys. Res. 111, D21116 https://doi.org/10.1029/2005JD006821.